APPENDIX A

FINAL PROJECT SUMMARY REPORT

PROJECT IDENTIFICATION INFORMATION

1. BUSINESS FIRM AND ADDRESS
JENTEK Sensors, Inc.
110-1 Clematis Avenue
Waltham, MA 02453

2. DOT SBIR PROGRAM
2006 PHASE I

3. DOT CONTRACT NUMBER
DTRT57-07-C-10005

4. PERIOD OF PERFORMANCE
From December 1, 2006 **To** May 31, 2007

5. PROJECT TITLE

High Resolution Electromagnetic Imaging and Decision Support for Pipeline Life Management

SUMMARY OF COMPLETED PROJECT

In this study, JENTEK® Sensors, Inc. has successfully adapted the MWM-Array® technology for the detection and mapping of stress corrosion crack (SCC) clusters in oil and gas transmission pipelines. Results indicate that MWM-Array measurements compare favorably with magnetic particle inspection (MPI), which is the industry standard method for characterizing SCC. The MWM-Array technology is expected to offer enhanced capabilities over MPI in inspection speed, data analysis, data archiving, and cost. This Phase I SBIR has had unusual success, considering the short duration of the program. Within the Phase I time period, JENTEK and our subcontractor RTD Quality Services, Inc. have secured funding from three major oil pipeline operators to validate the MWM-Array performance for transition of SCC mapping capability to the field this year.

Major accomplishments of this Phase I effort include:

- Demonstration of enhanced high resolution mapping of SCC clusters
- Detection, imaging and location of SCC colonies through pipeline coatings
- Development of a tool for automated length estimation for cracks
- Development of a tool for automated evaluation of crack interactions
- Development of preliminary methods to suppress sources of false indications
- Demonstration of preliminary capability to provide MWM-Array surface profilometry for physical damage

JENTEK has had substantial success transitioning SBIR funded technology in the aerospace and defense sectors, and we anticipate similar success for the characterization of SCC in pipelines. We have also identified several related applications of interest for which the MWM-Array technology should offer substantial advantages.

APPROVAL SIGNATURES

1. PRINCIPAL INVESTIGATOR/ PROJECT DIRECTOR (Typed)	2. PRINCIPAL INVESTIGATOR/ PROJECT DIRECTOR (Signature)	3. DATE
Neil J. Goldfine, Ph.D.		

Department of Transportation
Phase I SBIR Contract Number DTRT57-07-C-10005

Effective Date: December 1, 2006 through May 31, 2007

Research Topic No. 06-PH1

High Resolution Electromagnetic Imaging and Decision Support for Pipeline Life Management

May 31, 2007

Submitted to

Mr. James Merritt
US DOT / Office of Pipeline Safety
R&D Program Manager
HRDO-04, Room T-204
793 Countrybriar Lane
Denver, CO 80129

Preface

This Phase I SBIR has had unusual success in a very short period of time. Within the Phase I time period, JENTEK® Sensors, Inc. and our subcontractor RTD have secured funding from three major oil pipeline operators to transition the JENTEK MWM-Array® stress corrosion crack (SCC) cluster mapping capability to the field this year. The funding has already begun in parallel with the completion of this Phase I effort, and preliminary results from this effort are included in this final report. The goals of this transition funding are to obtain approval for the technology transition by the fall of 2007 and for RTD to begin offering MWM-Array SCC mapping as a replacement for MPI by the end of 2007 or early 2008.

This rapid transition is possible because of the advances made under this Phase I funding to enhance the MWM-Array imaging capabilities for SCC mapping. The initial application being transitioned requires the removal of the pipeline protective coatings. However, this Phase I effort has also demonstrated preliminary capability to detect SCC clusters through these coatings.

We strongly recommend that this program continue to a Phase II funded effort. Preliminary investigations of crack depth measurement capability indicate that this should be possible with low frequency MWM-Arrays. In Phase II, we recommend that the focus is on crack depth estimation using low frequency methods and on enhancement of resolution and speed for through-coating inspection capabilities. We are highly confident that these practical tools can be successfully commercialized and that, as in Phase I, we will rapidly move these additional technologies to field implementations. Without the Phase II funding it will be difficult to reach the full capability offered for this SCC mapping opportunity. Also, we anticipate that matching funding will be available through PRCI and the current joint funded program participants.

The major accomplishments of this Phase I effort include:

- Demonstration of enhanced high resolution mapping of SCC clusters
- Detection, imaging and location of SCC colonies through coatings
- Development of a tool for automated length estimation for cracks
- Development of a tool for automated evaluation of crack interactions
- Development of preliminary methods to suppress sources of false indications
- Demonstration of preliminary capability to provide MWM-Array surface profilometry for physical damage

In addition, and perhaps most importantly, JENTEK has developed new relationships with pipeline operators, service providers and oil companies. JENTEK has had substantial success transitioning SBIR funded technology in the aerospace and defense sectors, and we anticipate similar success for pipelines. We have also identified several related applications of interest for which the MWM-Array technology should offer substantial advantages. These related opportunities include:

From the outside diameter (O.D.)

1. imaging of surface corrosion through insulation (2-4 inches thick)
2. imagine of internal corrosion through insulation (2-4 inches thick)
3. imaging of internal and external corrosion through concrete under water

From inside diameter (I.D.), using a pigging platform

4. imaging of SCC on the O.D.
5. imaging of SCC on the I.D., e.g., for ethanol transport lines
6. imaging of external corrosion
7. imaging of internal corrosion, including through corrosion products
8. imaging of mechanical damage

We strongly recommend that each of these efforts be funded and we anticipate substantial industry participation. Separately, we have strong interest and funded efforts ongoing for drilling rigs (e.g., drill pipe inspection) that will benefit from continuing this SBIR funding.

Introduction

This Phase I SBIR focused on detection and imaging of SCC on the outside diameter surface of oil and gas pipelines as a replacement for Magnetic Particle Inspection (MPI). This includes detection, length and depth sizing, and obtaining positional information. The capability to automatically map crack clusters, estimate crack lengths and compute likely crack interactions (that accelerate crack growth) has been demonstrated. The capability to estimate crack depth has also been investigated.

Immediate value from these developments is anticipated through transition to the field this year of the crack cluster mapping and crack length determination capabilities. Crack depth estimation requirements were defined to include lower frequency operation than is currently possible with JENTEK's commercial product. However, JENTEK is developing a lower frequency instrument that will be available to support the recommended Phase II effort. For 1/2–in. thick pipeline, the requirement is to measure crack depths so that cracks less than 10 % of the wall thickness can be separated from deeper cracks, and cracks greater than 30% and 60% of the wall thickness can be identified. These are representative values expressed at the recent PRCI SCC review meetings in Calgary, which JENTEK attended at RTD's invitation. Thus, in the recommended Phase II effort, crack depth estimation should be a major focus.

The tasks completed under this Phase I SBIR program are listed below:

Task 1: Problem definition.

Task 2: Sample acquisition.

Task 3: Evaluate capability to perform high-resolution imaging of SCC colonies.

Task 4: Evaluate capability to detect SCC colonies through coatings.

Task 5: Evaluate capability to provide significantly enhanced characterization of pipeline coatings.

Task 6: Evaluate methods for integration of NDE data into pipeline life management programs.

Task 7: Investigate other life management opportunities for MWM-Arrays and IDED-Arrays.

Task 8: Final Report.

The following sections provide details of the Phase I accomplishments.

Comparison to existing technology

The industry standard for the characterization of SCC is magnetic particle inspection (MPI). To perform an inspection, the coating on the pipe is removed and the pipe is cleaned to provide a fresh metal surface for the inspection. With this method, a technician measures some critical metrics, such as the maximum crack length, average crack length, maximum interlinking crack length, circumferential separation between cracks, axial separation between cracks, the dimensions of the cluster, and interaction between clusters. These measurements are typically made using a ruler. The maximum depth of the clusters is then estimated using step-wise grinding. This information is then used to assess the safety of the pipeline. After the inspection, the pipe is cleaned again, and the coating is reapplied.

Accurate manual measurement of crack parameters is an extremely tedious, if not impossible, task due to the large number of closely spaced cracks that may be present in a cluster. In addition, photographing indications is the only way to review results at a later date, so the documentation and checking of results at a later date is quite difficult.

JENTEK's MWM-Array technology enables many benefits over the existing MPI technology, including automatic determination of crack length and crack interaction, electronic storage and retrieval of measurement data, and also potentially the ability to perform preliminary inspection of the pipeline without having to remove the coating. In order to compare the MWM-Array technology to MPI, we have focused on the following areas:

1. High-resolution imaging of cracks and clusters of cracks.
2. Automatic crack length and crack location logging.
3. Data processing algorithms to automatically estimate crack interaction.
4. Detection of cracks through coatings.
5. Lower-resolution rapid scanning for wide areas to identify regions of interest.
6. Suppression of false indications.
7. Matching or exceeding MPI performance.

Description of pipeline samples with SCC used in this SBIR effort

Multiple samples of pipeline sections containing regions of SCC were provided for this SBIR program by JENTEK's subcontractor, RTD Quality Services (RTD). These pipeline sections are described below and shown in the following figures.

1. Plate, RTD #10407, is generally triangular in shape with a slight double curvature, and is approximately 18 x 13 in. (see Figure 1)
2. Plate, RTD #10413, is 7 x 12 in. with a single gradual curvature (see Figure 1).

These two plates are 0.33 in. thick steel, and contain numerous SCC clusters.

Samples from the ongoing, transition effort were also made available for this program. This study provided eight plates cut from various transmission pipelines, ranging in size from 8 x 18 in. to 20 x 30 in. Three of these plates are shown in Figure 2, Figure 3, and Figure 4.

Figure 1. Photograph of two pipeline sections with SCC received from RTD Quality Services, Inc.

Figure 2. Photograph of "Plate-01" from the transition study.

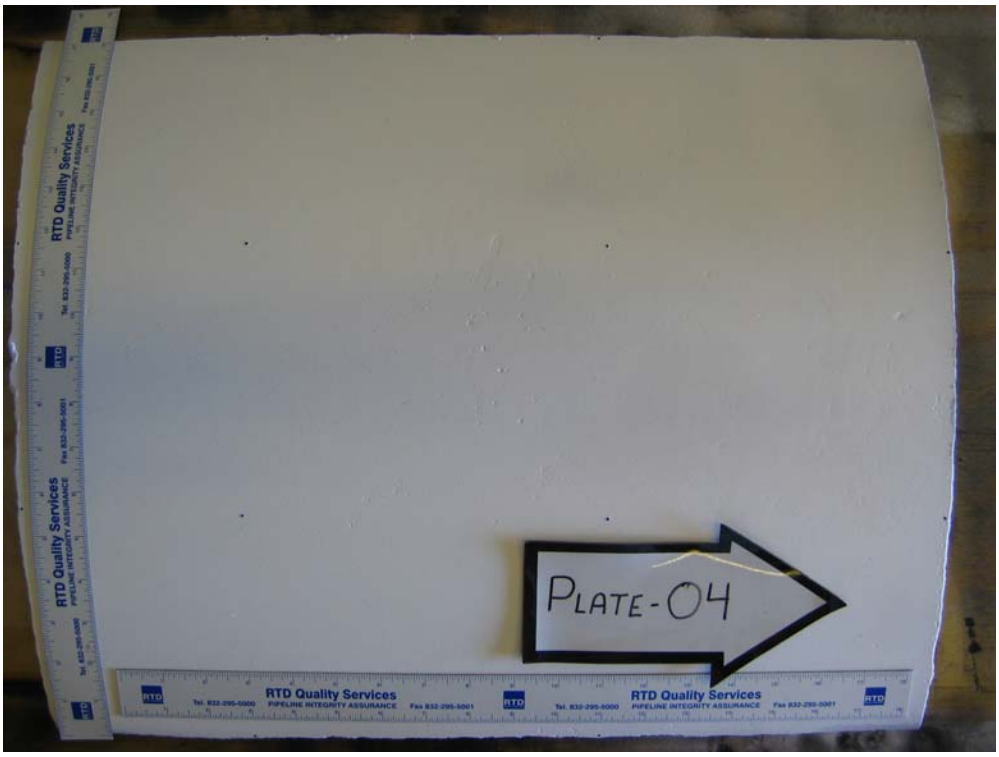

Figure 3. Photograph of "Plate-04" from the transition study.

Figure 4. Photograph of "Plate-08" from the transition study.

Results of MWM-Array measurements: high resolution imaging of SCC

Available JENTEK MWM-Array sensors were used to scan the triangular-shaped plate. An MWM-Array FA24 was used for broader area scans (discussed in a later section), and an MWM-Array FA28 was used for the high resolution scans. These sensors are shown in Figure 5. For the high-resolution FA28 measurements, an excitation frequency of 125 kHz was provided by the drive, and simultaneous measurements were continuously acquired by the array of 37 sensing elements as the sensor was moved across the part. Raw impedance data are converted to the property value measurements of conductivity and lift-off (the distance between the sensor and material). Conductivity measurements are used to detect/map the cracks. Lift-off measurements confirm that scans are performed within an acceptable range of sensor-material distance; they can also provide a measure of coating thickness and/or surface topology. The conductivity and lift-off are computed in real-time using JENTEK's patented multivariate inverse methods, illustrated in Figure 6. For these scans we used a two-unknown (grid) method to simultaneously solve for conductivity and lift-off, and assumed the magnetic permeability was constant. This assumption is known to be incorrect, but for the data acquired to date, it has been satisfactory for the detection and characterization of SCC. In Phase II a 3-unknown (lattice) methods to simultaneously solve for conductivity, permeability, and lift-off should be investigated to determine if susceptibility to SCC and residual stress distributions can be mapped along with the SCC clusters.

The setup used to perform the scans is shown in Figure 7. The manual scanning cart used to perform the measurements was equipped with an encoder to obtain positional information with the measurements. The sensor was backed with foam so that it would conform to the curvatures of the plate, and registration between the multiple scans was achieved by laying on top of the plate a 0.010 in. thick Mylar sheet that had lines drawn on it to mark the location of each scan. Conductivity images of the full sample plate were achieved by combining the data from multiple adjacent scans automatically using JENTEK's GridStation software.

Results of the high resolution FA28 scans of the triangular part are shown in Figure 8. Data are presented as effective conductivity maps of the material, and cracks appear as regions of low conductivity. The images reveal large regions where SCC has occurred, and discrete cracks can readily be identified. The measurement data are presented here in two color schemes. In the spectrum color scheme, conductivity values are presented in a continuous color scale, and in the grey-red threshold color scheme, the red regions are locations on the plate where the effective conductivity is lower than a specified value. The two color schemes can be used by the operator to obtain more information from the images than available in the two-color images.

Also shown in Figure 8 is a corresponding lift-off image, showing the distance between the sensor and the sample during these scans. The recording of lift-off provides not only surface topology information, as described later, but also ensures that the lift-off range is with in an acceptable range to achieve the desired crack detection sensitivity and sizing accuracy. The green image confirms that these measurements were within the acceptable lift-off range. Note that as each scan is performed, an image of the scan appears instantly in JENTEK's GridStation software environment, providing immediate feedback to the operator. Furthermore the software can easily archive this digital data for historical records and convert crack detections into logs of crack lengths and locations, as described below.

Figure 9 shows a larger view of the same conductivity scan image. A photograph of MPI results from the same area, provided by RTD, is shown in Figure 10. Shown in Figure 11 is the same area imaged using a thresholded color scheme where the threshold is set at a conductivity value of 2.7 %IACS. This threshold image does not show some of the smaller (circled) cracks shown in the MPI photograph of Figure 10. However, the smaller cracks are all visible in the spectrum image of Figure 9.

When the threshold is increased to 3.5 %IACS, the smaller cracks become visible as shown in Figure 12. It is important to note that the threshold value appropriate for SCC characterization in pipelines is currently being determined under the ongoing transition program by obtaining feedback from both RTD and the pipeline operators on their current MPI practice.

Figure 13 and Figure 14 show FA28 conductivity scan images of "Plate-01" and "Plate-04" from the transition study. These plates had been cut from pipelines, and SCC is present in both plates. Figure 15 shows a scan image from "Plate-08" of the transition study. In this plate the SCC occurred in a region adjacent to the longitudinal weld in the pipe. Though not known for certain, it is likely that a wrap-type coating that was applied to this pipeline was "tented" over the surface adjacent to the weld,which is a condition that is often observed in the field. In such a condition, any holiday in the coating can result in the ingress of an environment amenable to SCC. It can also result in puddling of moisture along the edge of the "tented" (or disbonded) region on either side of the weld. Such a situation appears to have occurred in Plate-08, resulting in a thin linear region of material loss due to corrosion at the edges of the disbond and SCC occurring between these regions and the weld. In Figure 15, this thin region of material loss is evident in the lift-off image, and the SCC is evident in the conductivity image. This illustrates the potential of the MWM-Array to simultaneously map surface material loss from corrosion and detect SCC in the same scan pass.

Figure 16 is a 3-D presentation of the same Plate-01 conductivity data shown in Figure 13. This type of image can be used to better visualize discrete cracks within a cluster, especially when the cracks are so closely spaced that the usual spectrum color or threshold color images show them as one large indication. It is important to note that the z-axis scale in the 3-D image is sensor response, not crack depth. Though the two are related for shallow cracks, there are other factors such as crack width that can affect sensor response. For deeper cracks, at the frequencies used here, the MWM-Array does not have sufficient depth of sensitivity to provide a reliable measure of crack depth. This would be addressed in the recommended Phase II.

Automatic Crack Sizing and Mapping

Under this SBIR program and JENTEK IR&D, we have developed preliminary signal processing algorithms to automatically determine crack length and crack spacing from the digital data acquired with MWM-Array scans. Figure 17 presents the same data as was shown in Figure 9, but this time with a simple threshold value of 3.5%IACS applied, and without the averaging of neighboring pixels, which was done for Figure 11 and Figure 12. Hysteresis thresholding, a method which uses two thresholds, was then applied to the data. All pixels corresponding to conductivities below the lower threshold are set to 1 (these pixels satisfy both thresholds). Those above the higher threshold are all set to zero. For the pixels with conductivities between the two thresholds, those that are connected to pixels lower than the lower threshold are set to 1, but only if they are connected through pixels with conductivities all below the upper threshold. The rest of the pixels with conductivities between both thresholds are set to zero. The results are shown in Figure 18. Some of the noise that appears in simple thresholding images is filtered out when hysteresis thresholding is performed.

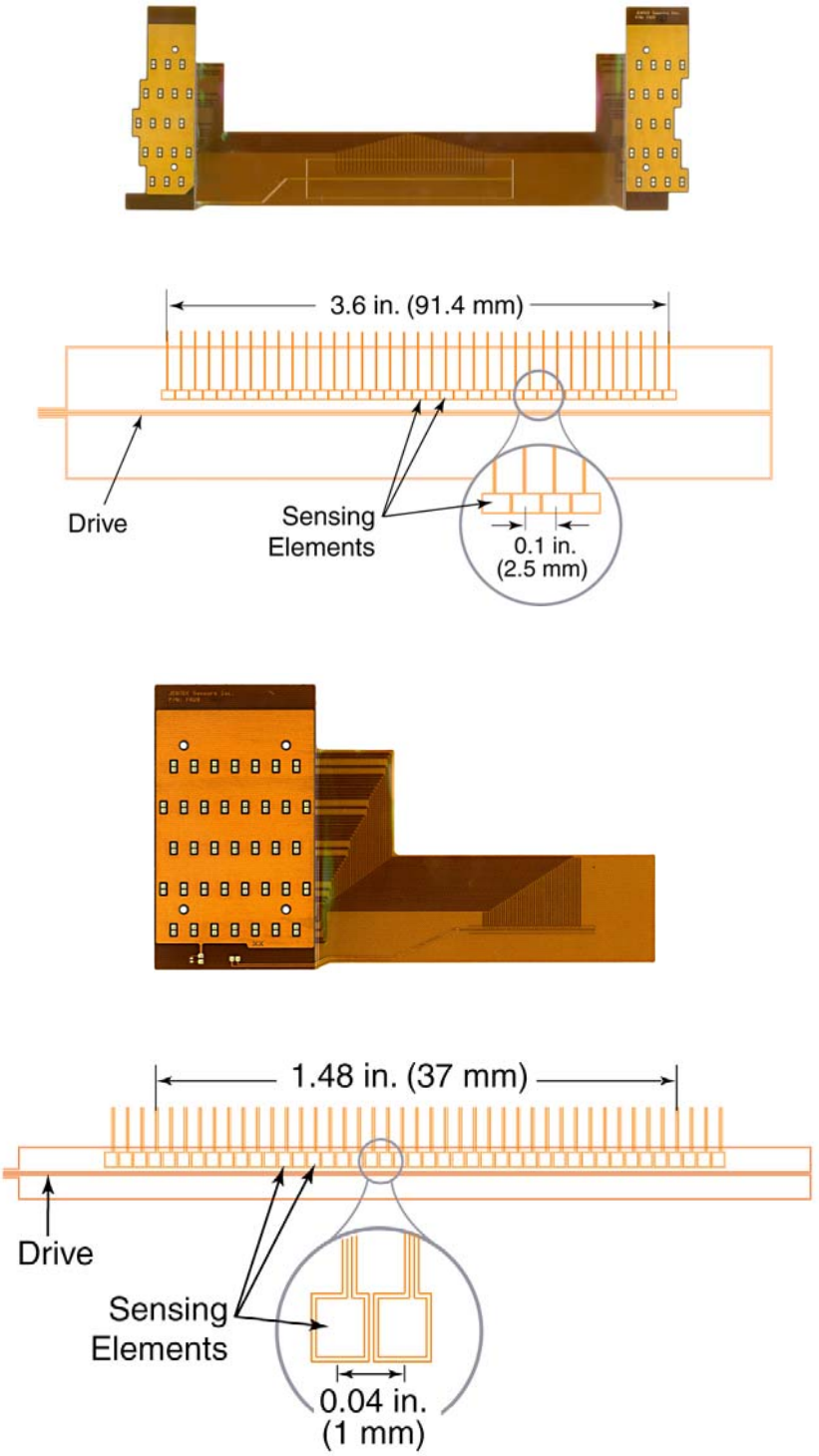

Figure 5. (Top) The MWM-Array FA24 sensor used for broader area scans. (Bottom) The MWM-Array FA28 sensor used for high resolution scans.

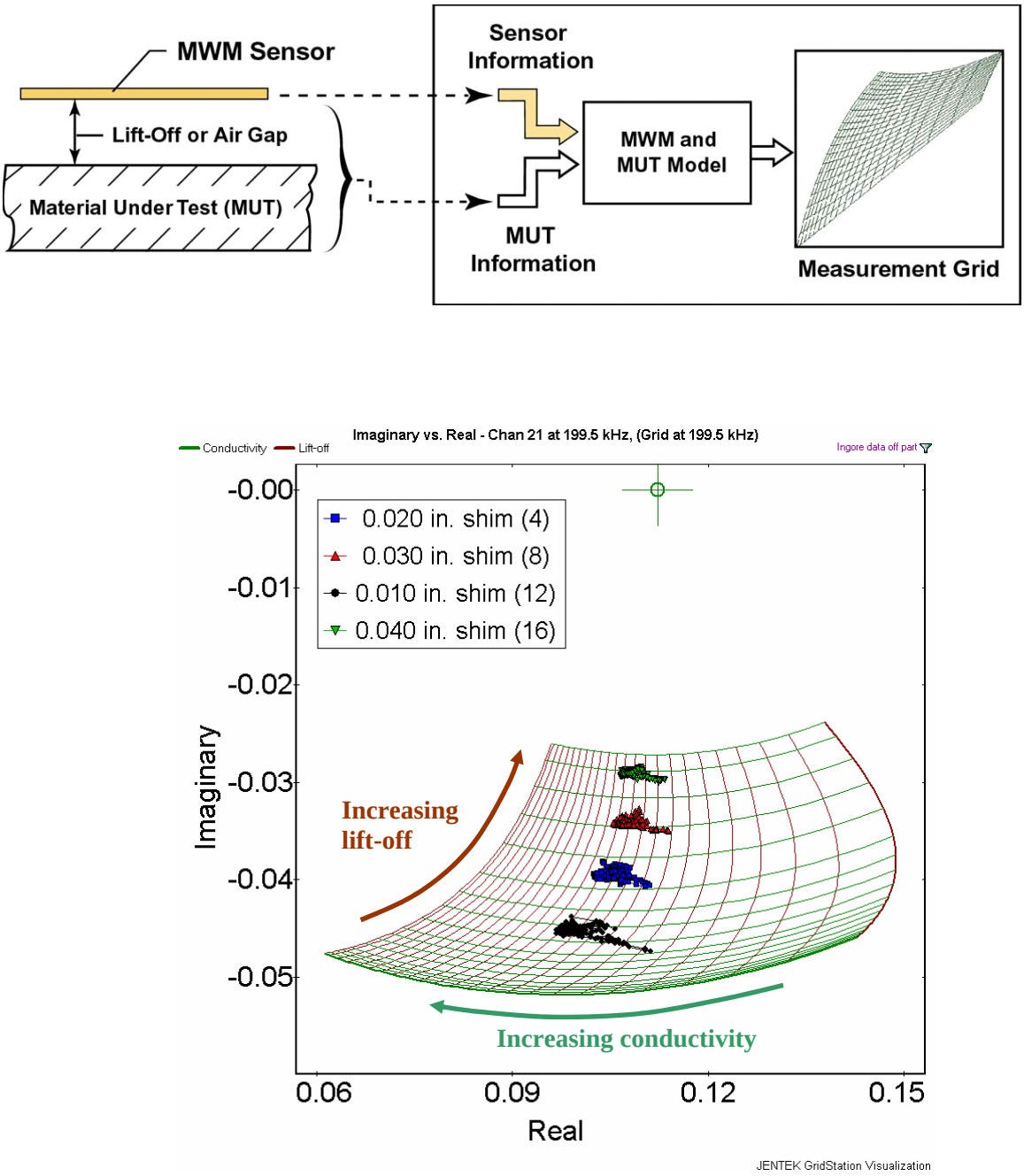

Figure 6. (Top) Illustration showing how information about the sensor and the material under test are used to construct a precomputed database, or Measurement Grid, which is used to convert the sensor response into property values such as conductivity (σ) and lift-off (h). (Bottom) A σ-h Measurement Grid used in scans of the steel specimens with SCC. Plotted are data from one of the FA24's thirty six sensing channels (channel 21) in scans performed with four different coating (shim) thicknesses. The data show how the GridStation independently measures the lift-off values while determining the material's conductivity without significant influence from varying lift-off.

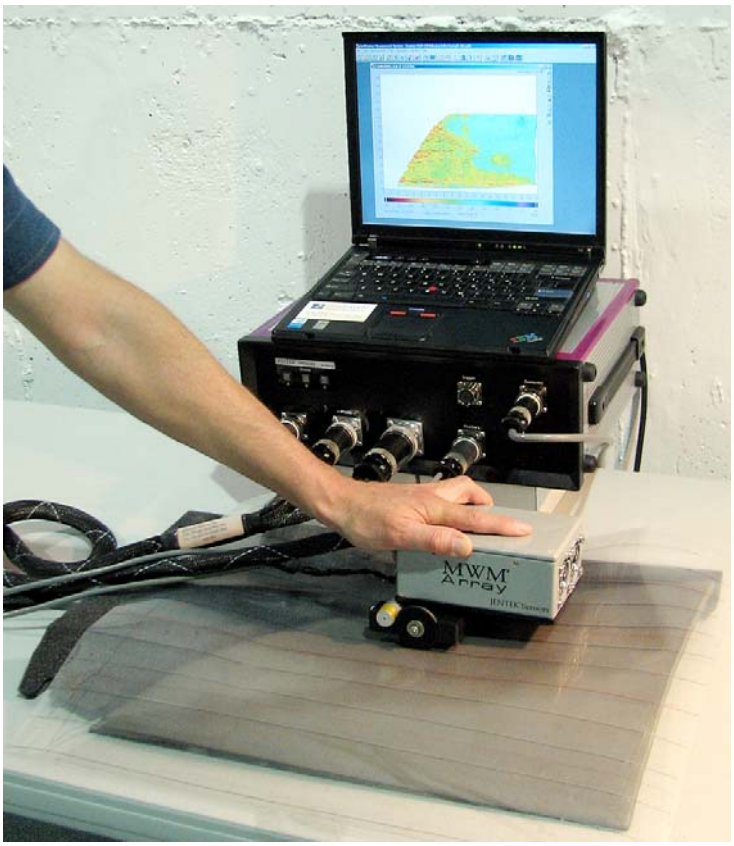

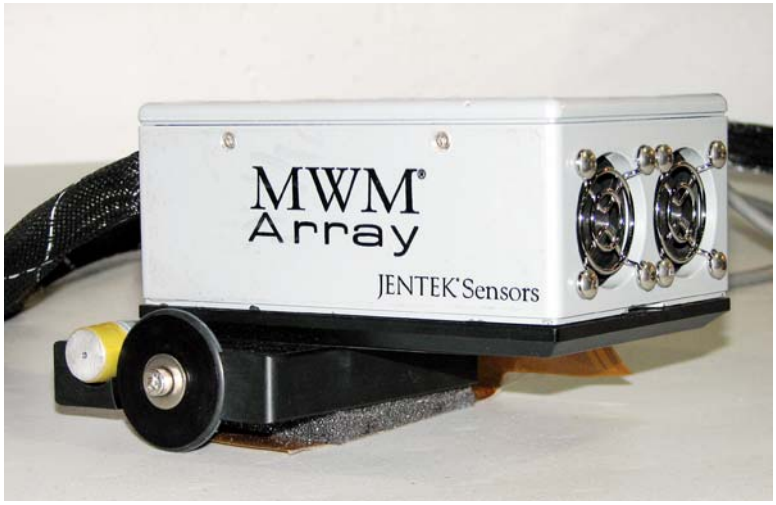

Figure 7. (Top) Photograph of the setup used to perform manual scans of the triangular plate. Shown are JENTEK's 39-Channel impedance instrument, host laptop computer, and the triangular RTD plate with a lined Mylar sheet laying on it to assist in registering the position of the multiple scans. (Bottom) Photograph of the probe electronics/scanning cart assembly showing the position encoder and foam-backed sensor, which conforms to the curvatures of the plate.

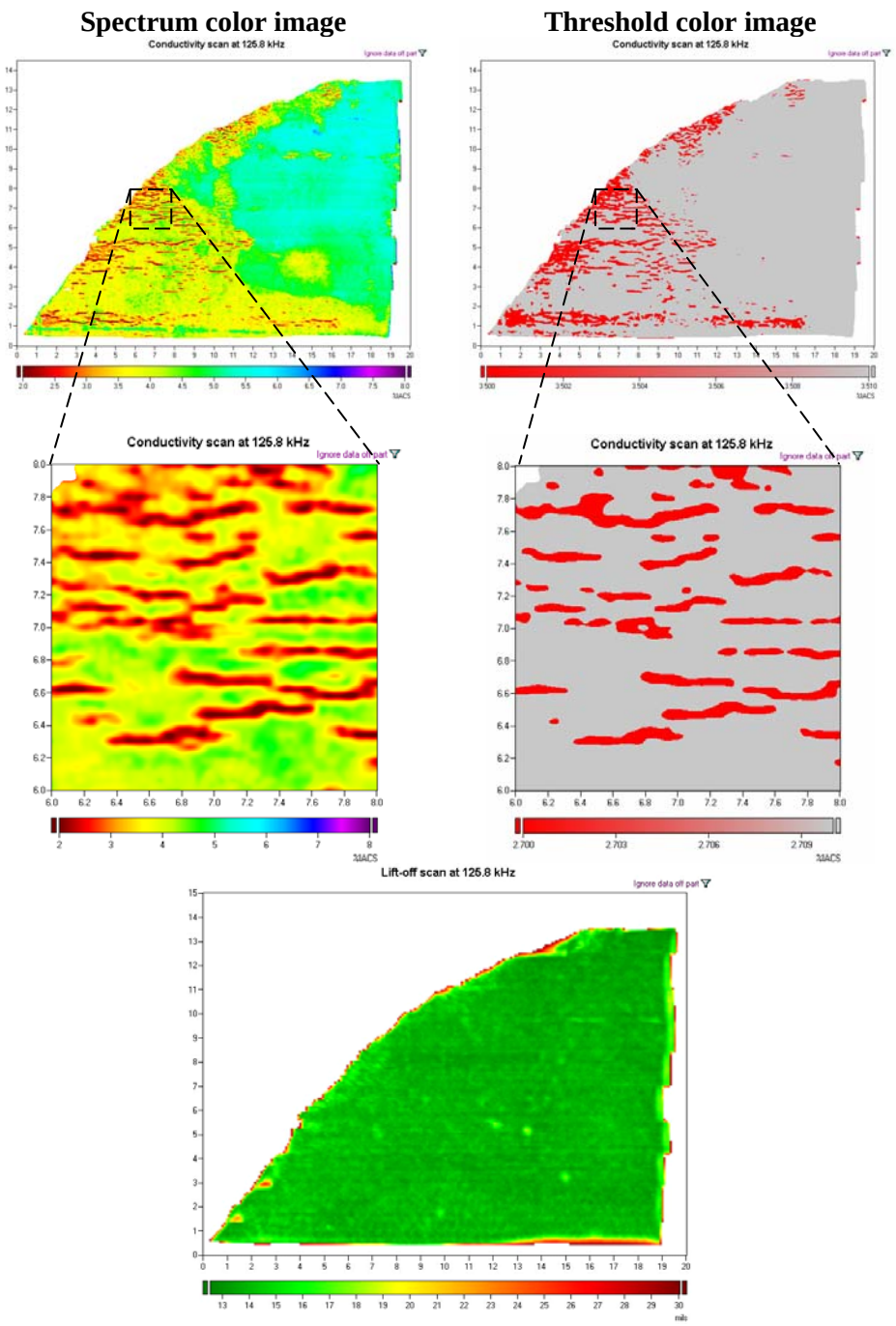

Figure 8. Conductivity and lift-off images of plate # 10407, which contains numerous stress corrosion cracks. The left pairing of images show the conductivity data in a spectrum color scheme, where variations in effective conductivity across the surface are presented in a continuous color scale. The right pairing of images show the same data using a threshold color scheme, in which red indicates where the effective conductivity is below a certain value. The bottom image shows the lift-off data, in which green indicates that the lift-off values are within a suitable range. X- and Y-axis units are inches.

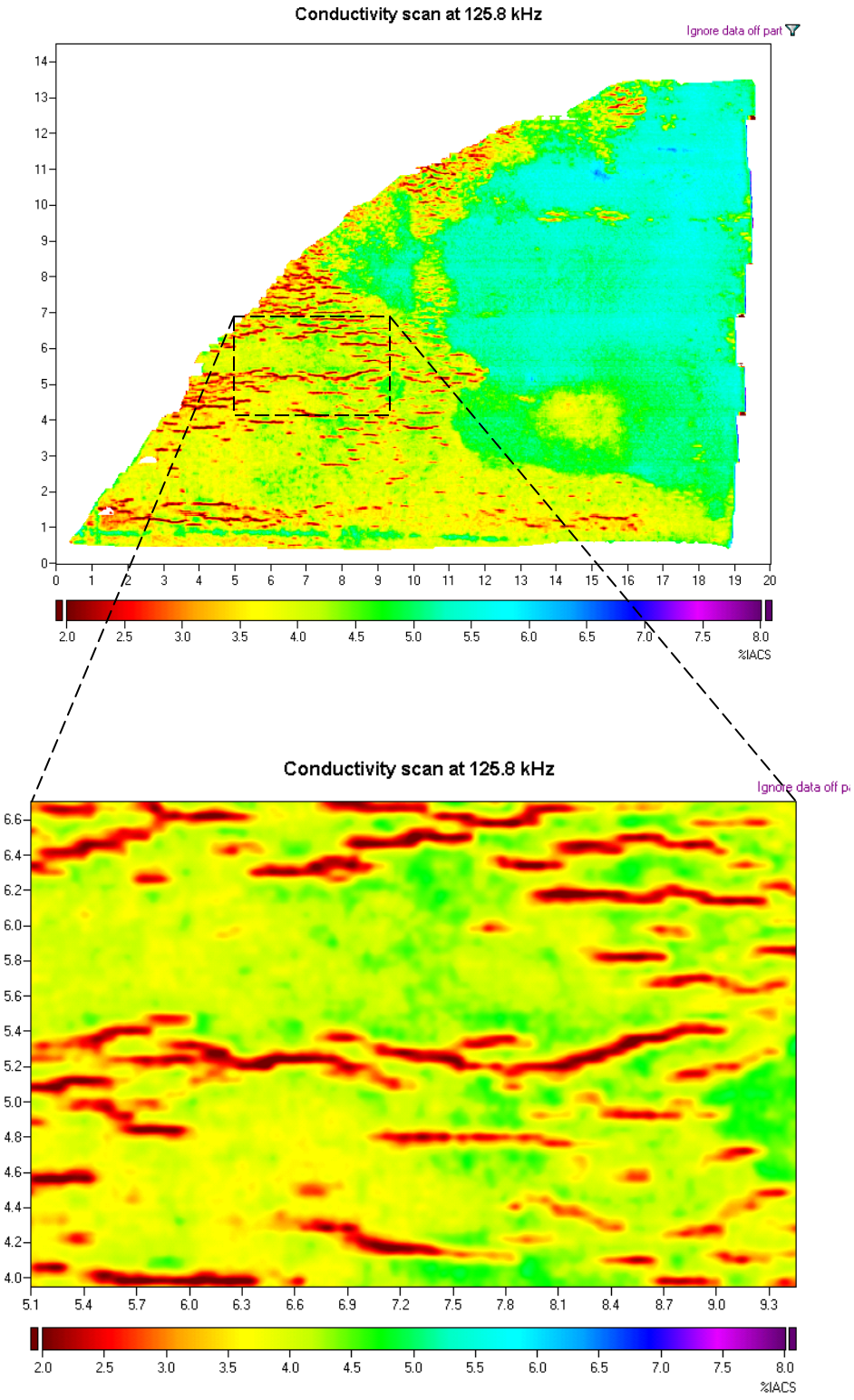

Figure 9. Expanded view of the FA28 conductivity data shown in Figure 8.

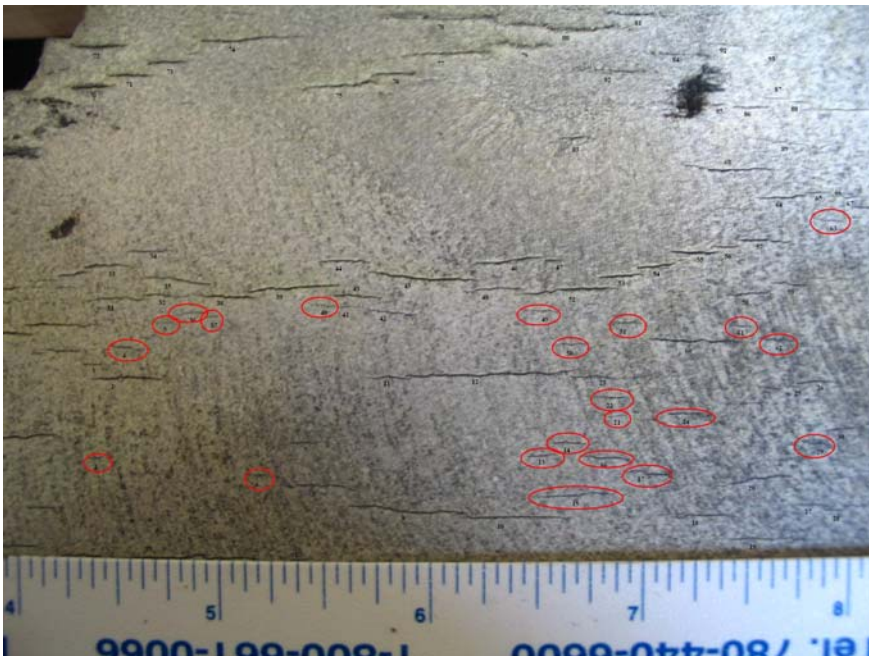

Figure 10. RTD's MPI results from the same area shown in Figure 9.

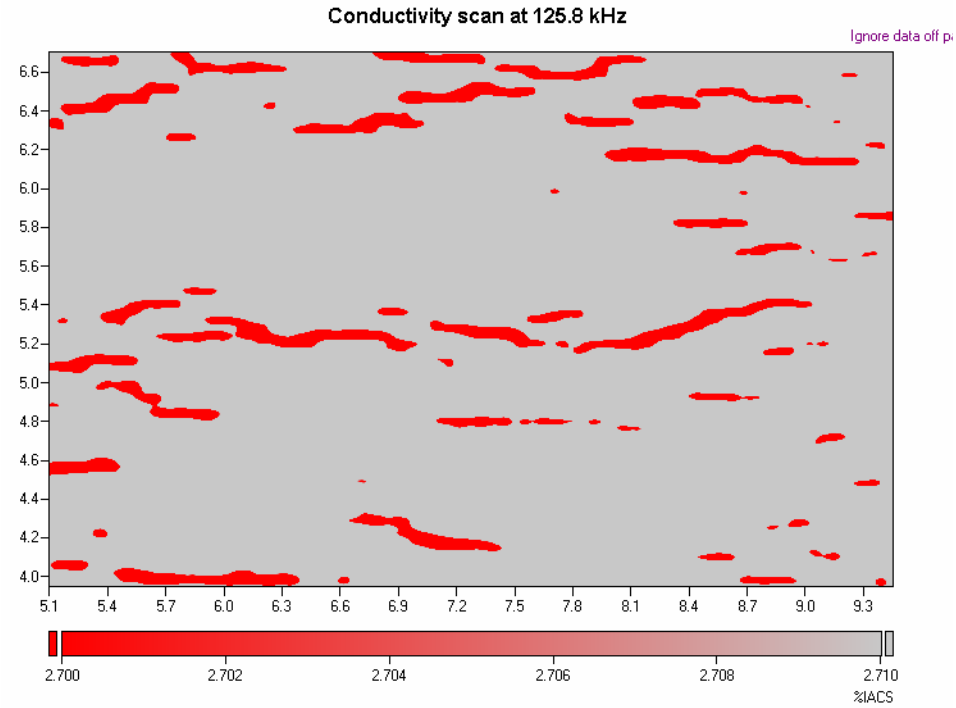

Figure 11. Thresholded FA28 scan image from the same area shown in Figure 9 and Figure 10, with the conductivity threshold set at 2.7 %IACS. The cracks in Figure 10 that are circled in red do not appear in this image, but do appear in the spectrum color image of Figure 9.

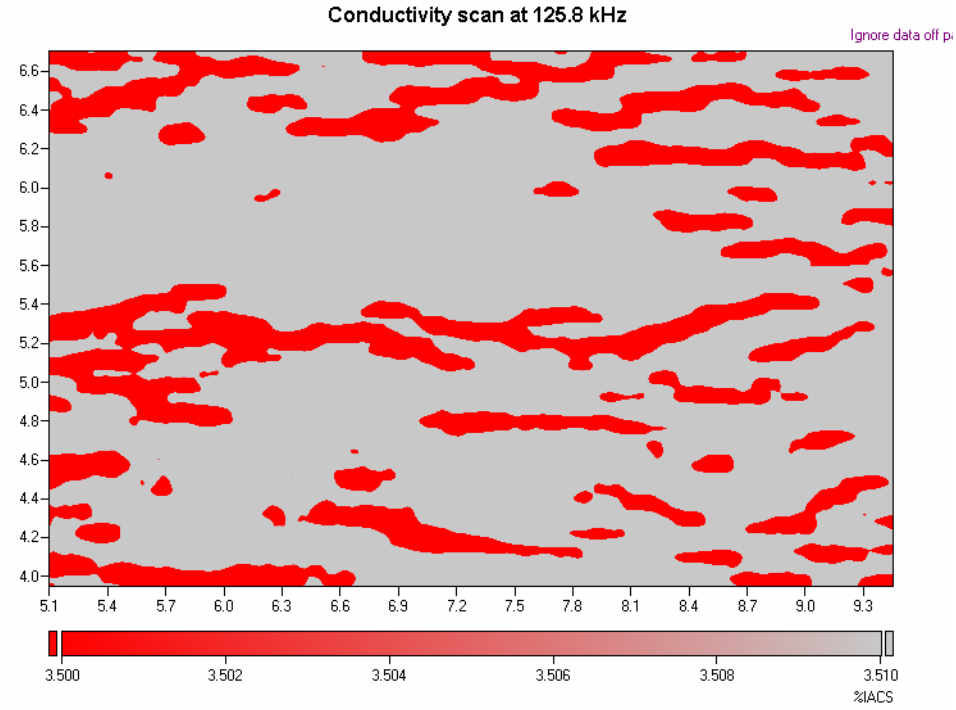

Figure 12. The same expanded view with the threshold set at 3.5 %IACS.

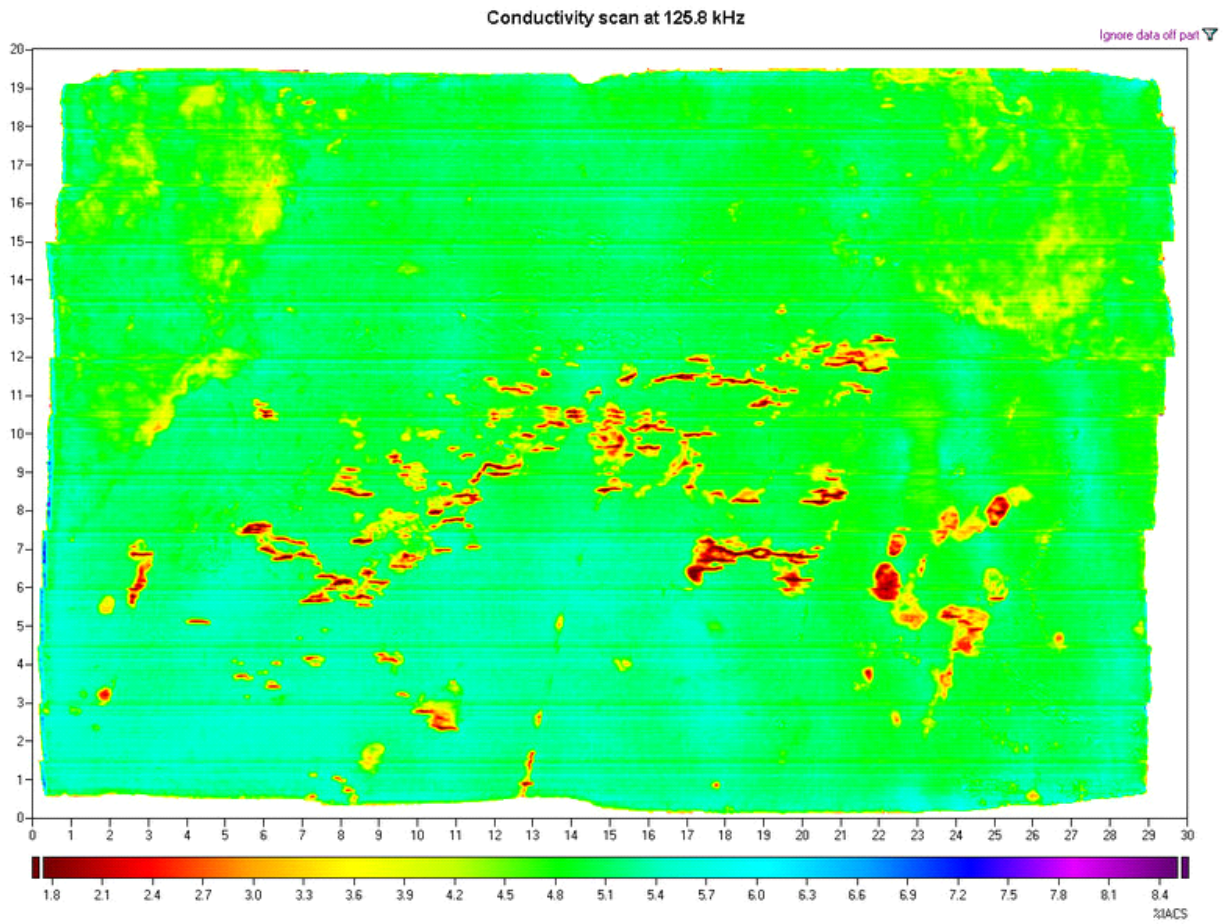

Figure 13. FA28 conductivity image of "Plate-01," shown in Figure 2. X- and Y-axis dimensions are inches.

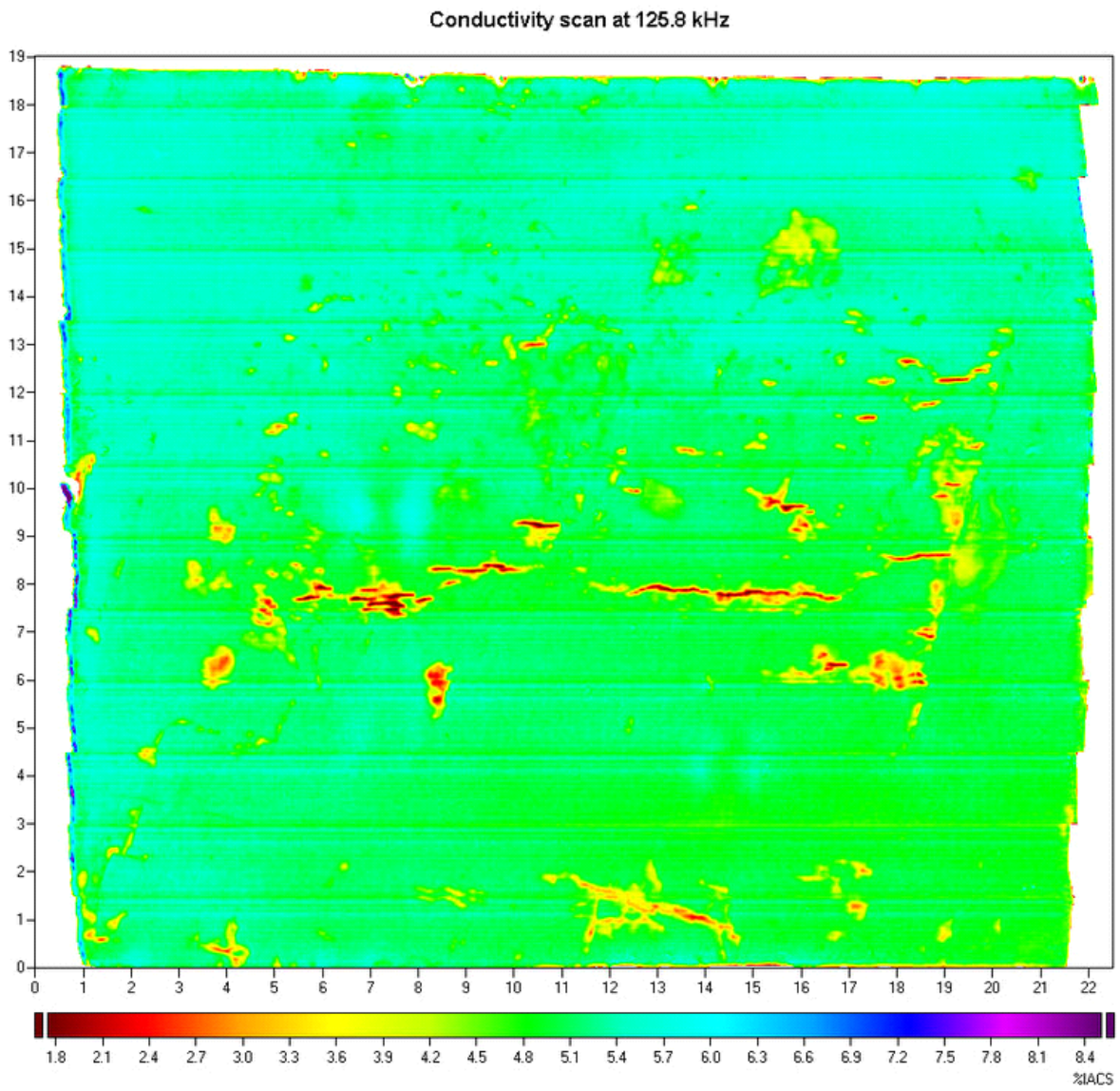

Figure 14. FA28 conductivity image of "Plate-04," shown in Figure 3. X- and Y-axis dimensions are inches.

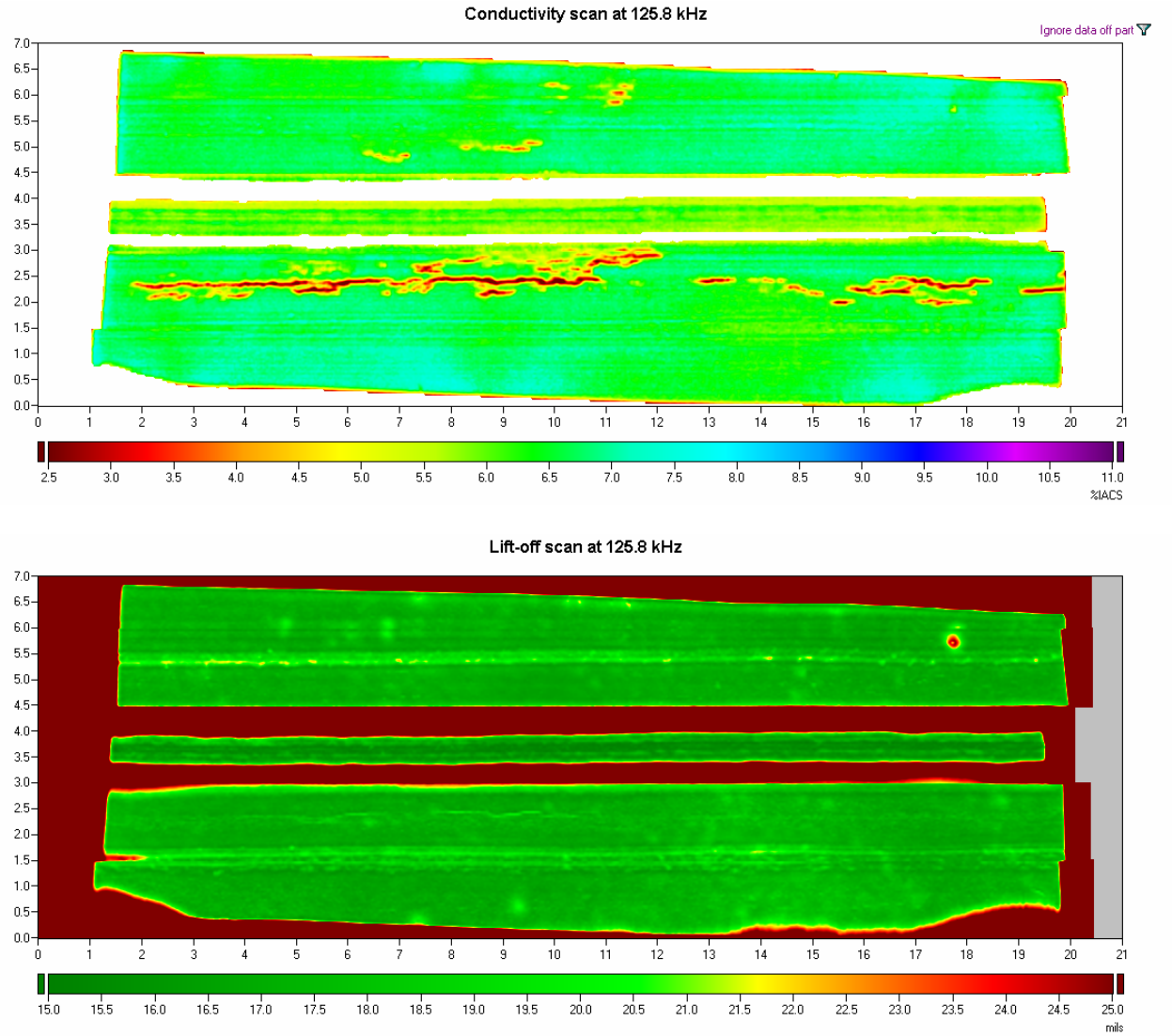

Figure 15. FA28 conductivity (top) and lift-off (bottom) scan images of "Plate-08," shown in Figure 4. The x and y-axis dimensions are inches. Note that the two major longitudinal white stripes in the conductivity image and the corresponding red stripes in the lift-off image are on either side of the weld crown where the sensor was not in contact with the toe of the weld. It was not our intention in these scans to characterize the weld, and thus no effort was made to fixture the sensor so that it would be in intimate contact with the toe of the weld.

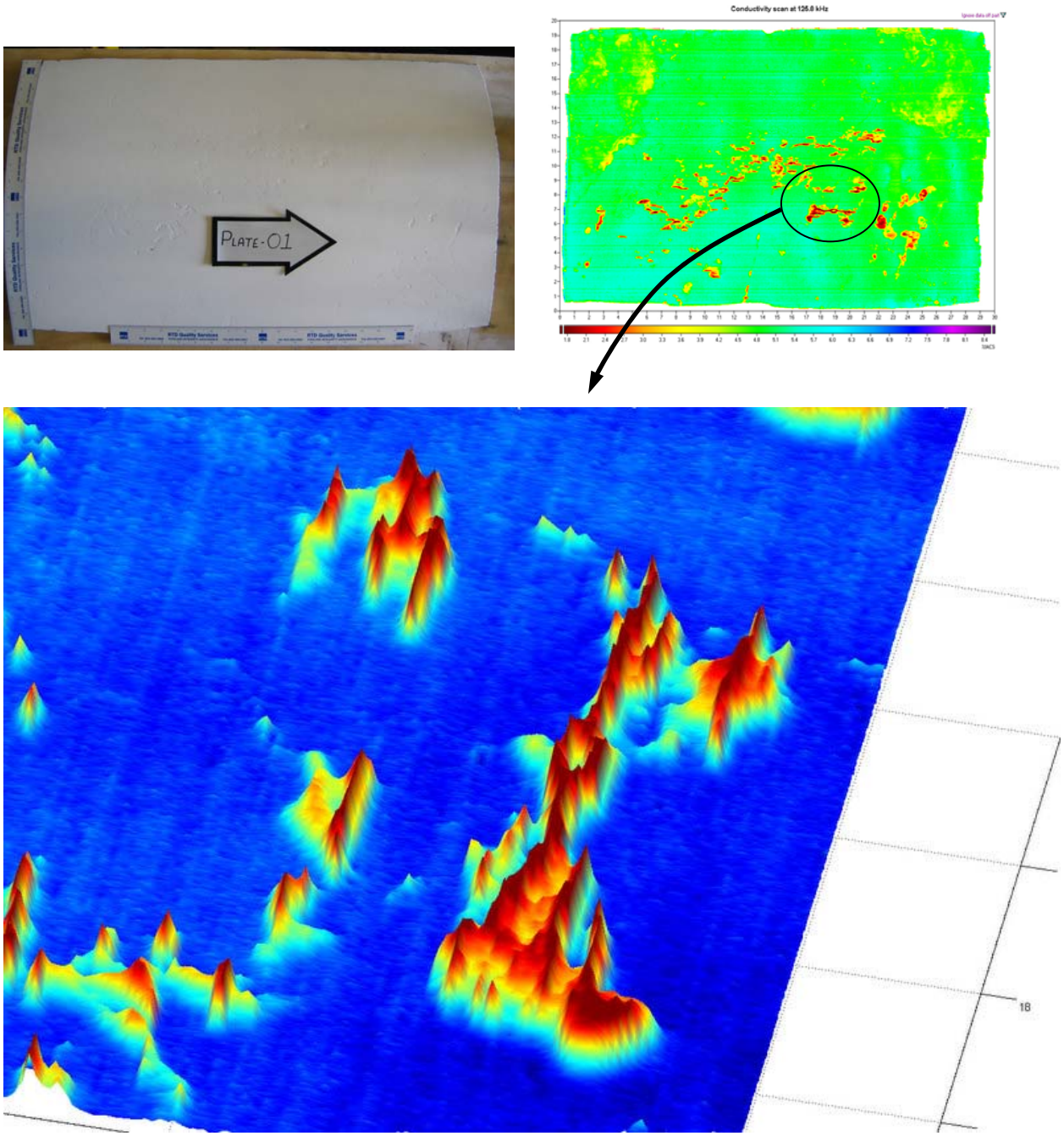

Figure 16. 3-D presentation of the same conductivity data shown in Figure 13. This type of image can be used to better visualize discrete cracks within a cluster, especially when the cracks are so closely spaced that the usual spectrum color or threshold color image shows them as one large indication. The z-axis scale in the 3-D image is sensor response, not crack depth.

Other methods for yielding digital crack images are also being investigated. Figure 19 shows the results of applying the Canny edge detection method to the scanned images, which is a gradient based method. By this method the edges of the cracks are highlighted, but the central region of the cracks is not included. This method may have the benefit of detecting cracks when the background conductivity or magnetic permeability of the steel varies across its surface, where simple thresholding might be difficult. Another hybrid method that combines thresholded data with the edge detection data was also investigated, the results of which are shown in Figure 20. This method combines the Canny edge detection method with thresholded data to produce a full, albeit broader, indication from each crack. Still another procedure that was investigated is high-pass (spatial) filtering of the data followed by thresholding. Results of this method are shown in Figure 21 and Figure 22. In this method a Gaussian filter is used before high-pass filtering to remove some of the high frequency noise.

These methods can automatically produce crack length and position information from MWM-Array scans. A useful output from these methods is a tabulated list of the cracks present in a region, such as the one shown in Table 1. In this example, MWM-Array scan data from a region of Plate-01, shown in Figure 23, were thresholded and filtered. The cracks in this region are sorted by axial length, and only cracks with an axial length greater than (an arbitrarily chosen) 0.010 in. are included. With such a table, an inspector can immediately locate cracks that have the greatest impact on the health of the pipeline to support decisions.

Automatic determination of crack interaction

Under this SBIR program and JENTEK IR&D, we have also developed preliminary methods for determining crack interaction. Processed thresholded data, in this case the high-pass filtered and thresholded data, is used as the input to the algorithm for determining interaction. Each identified crack is assigned an ID number, and the coordinates of the pixels that belong to it are stored. The coordinates of all cracks are examined, and cracks in close proximity are analyzed to determine if they satisfy a prescribed interaction criteria. For this analysis, the criterion used to determine whether cracks are interacting is given in
Figure **24**. The maximum and minimum x and y coordinates of each crack are determined, as well as the size of each crack, the diameter (of the circumscribing circle) of the crack, and the mean x and y coordinates. By knowing the ID numbers of a crack's neighbors, the neighboring cracks' coordinates and properties are also known. Figure 25 shows a representative image where each crack, or grouping of connected cracks, is assigned a unique color corresponding to its ID number. Figure 26 shows the results of the crack interaction algorithm where the crack colored brown is the crack under consideration. The interacting cracks, as determined by the algorithm are shown in tan.

Note that the thresholding algorithms used in the previous examples often interpret closely spaced cracks as interconnecting cracks when their signatures in the image overlap. In such cases, the algorithms may consider a cluster of cracks as one larger interconnected crack. This is not expected to be a concern because it occurs in cases where the cracks are so close together as to meet the interaction criterion, and thus they should most likely be considered to behave as one crack.

Imaging cracks through coatings

Coatings are routinely applied to oil and gas transmission pipelines to prevent contact of the steel with corrosive soil, bacterial, fungal, and moisture environments. The most widely used coating system today is fusion bonded epoxy (FBE). These coatings are typically applied at the factory, and can be 100 µm to 250 µm (0.004-0.01 in.) thick. An abrasion resistant overcoat (ARO), from 500 µm to several mm thick, is usually applied on top of the first layer of FBE for increased resistance to mechanical damage. Other coating systems that are widely used in transmission pipelines, especially older pipelines, include polyethylene wrap, coal tar enamel, or an enamel tape wrap. Coating methods are often combined. Overall coating thicknesses range from tens of mils for FBE and polyethylene coatings to 1/4-1/2 in. for the older coal tar coatings.

It would be of great interest to industry if the broad-area preliminary scans could be performed through coatings. Presently magnetic particle inspection (MPI) procedures require removal of the coating and cleaning of the pipe, and then a subsequent cleaning of the pipe followed by reapplication of the coating. If MMW-Array procedures are successfully developed, the coating would only need to be removed if SCC is detected and only at the locations where high resolution scans are to be performed. Eliminating the need to remove and reapply the coating over healthy regions of the pipeline could result in a significant reduction in time and cost.

A two-step approach has been investigated for performing MWM-Array inspection of oil and gas pipelines. First, a broad-area, lower resolution scan, ideally without coating removal, would be performed to identify regions where SCC might be present. Second, a high resolution scan would be performed, with the coating removed, in selected areas of interest that are identified based on the first scan. A broad area scan must be rapid enough for the scans over the large pipeline surface to be performed in a practical amount of time while sensitive enough to detect SCC colonies. Then the high resolution scans in the areas of interest would enable crack sizing and interaction determination.

To demonstrate the ability to detect cracks through coatings, the triangular RTD specimen was scanned using an FA24 MWM-Array sensor with various amounts of plastic sheeting placed between the sensor and the specimen. The larger sensing element size of the FA24 allows area scan rates about twice that of the FA28. Figure 27 shows the results from four scans, performed with 0.010, 0.020, 0.030, and 0.040 in. shims between the sensor and the specimen. These images show that there is little difference in the conductivity measurements acquired over this range of lift-off. These shims are typical of FBE and polyethylene wrap coatings. Thicker coatings are addressed below.

The FA24 is not as accurate for crack length determinations as the FA28. As shown in Figure 28, which is an FA24 conductivity image from scans of the triangular plate, the larger sensing element size of this sensor reduces the spatial resolution substantially. However, these results demonstrate the concept of broad area scans followed by high resolution scans. If a region of reduced conductivity is detected with a broad area FA24 scan, it would be further investigated with a high resolution scan.

To demonstrate the ability to detect cracks at higher lift-off values (i.e., thicker coatings), a much larger array was used to scan the same triangular plate. The sensor used for this test was the FA122, shown in Figure 29. This is a large linear array developed by JENTEK and tested under an SBIR Phase II program with the Navy for detecting and monitoring corrosion in aircraft. Again this sensor is not appropriately designed for this application, though it was the most appropriate sensor available for this Phase I effort. In the recommended Phase II effort, a modified sensor would be fabricated with a more appropriate winding construct. Nevertheless, as shown in Figure 30 the FA122 detected the regions of SCC through 0.130 in. of simulated coating.

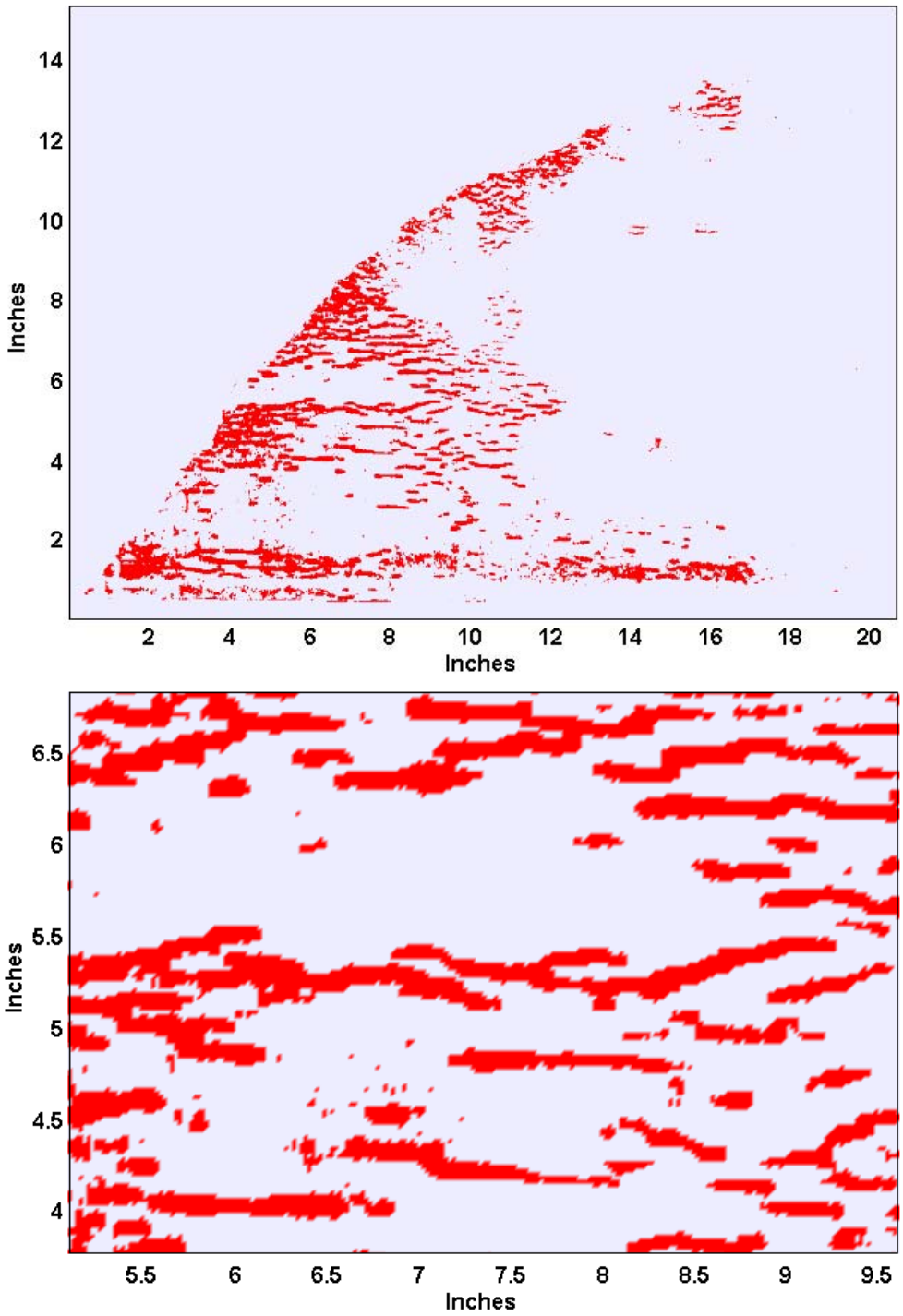

Figure 17. Thresholded FA28 scan data used for post processing (threshold = 3.5 %IACS). These are the same data shown in Figure 9. (Top) Conductivity image of the entire part. (Bottom) the same expanded area as shown in Figure 11, bottom and Figure 12.

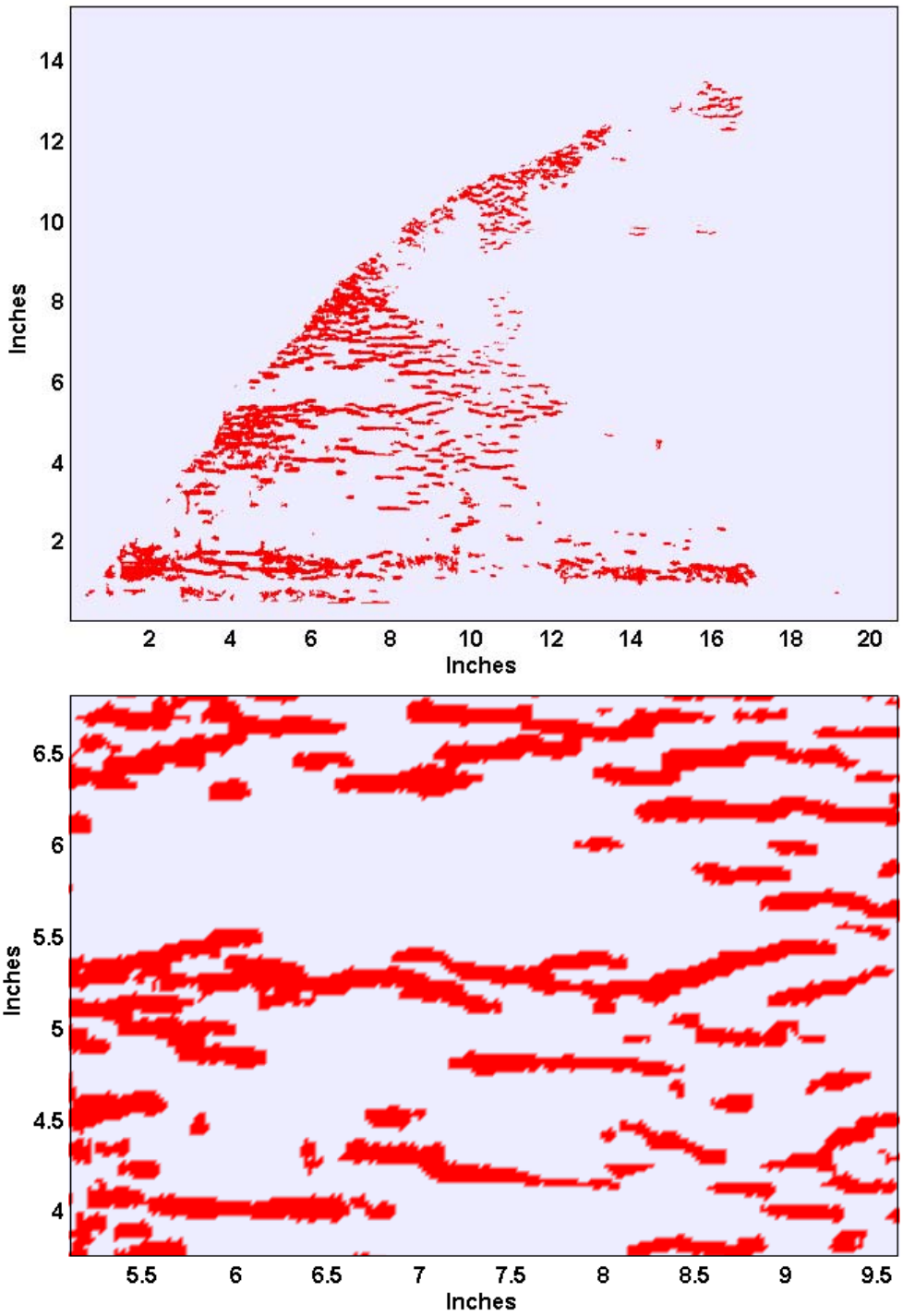

Figure 18. Hysteresis thresholded FA28 scan data. Lower threshold = 3.2 %IACS, upper threshold = 3.5 %IACS.

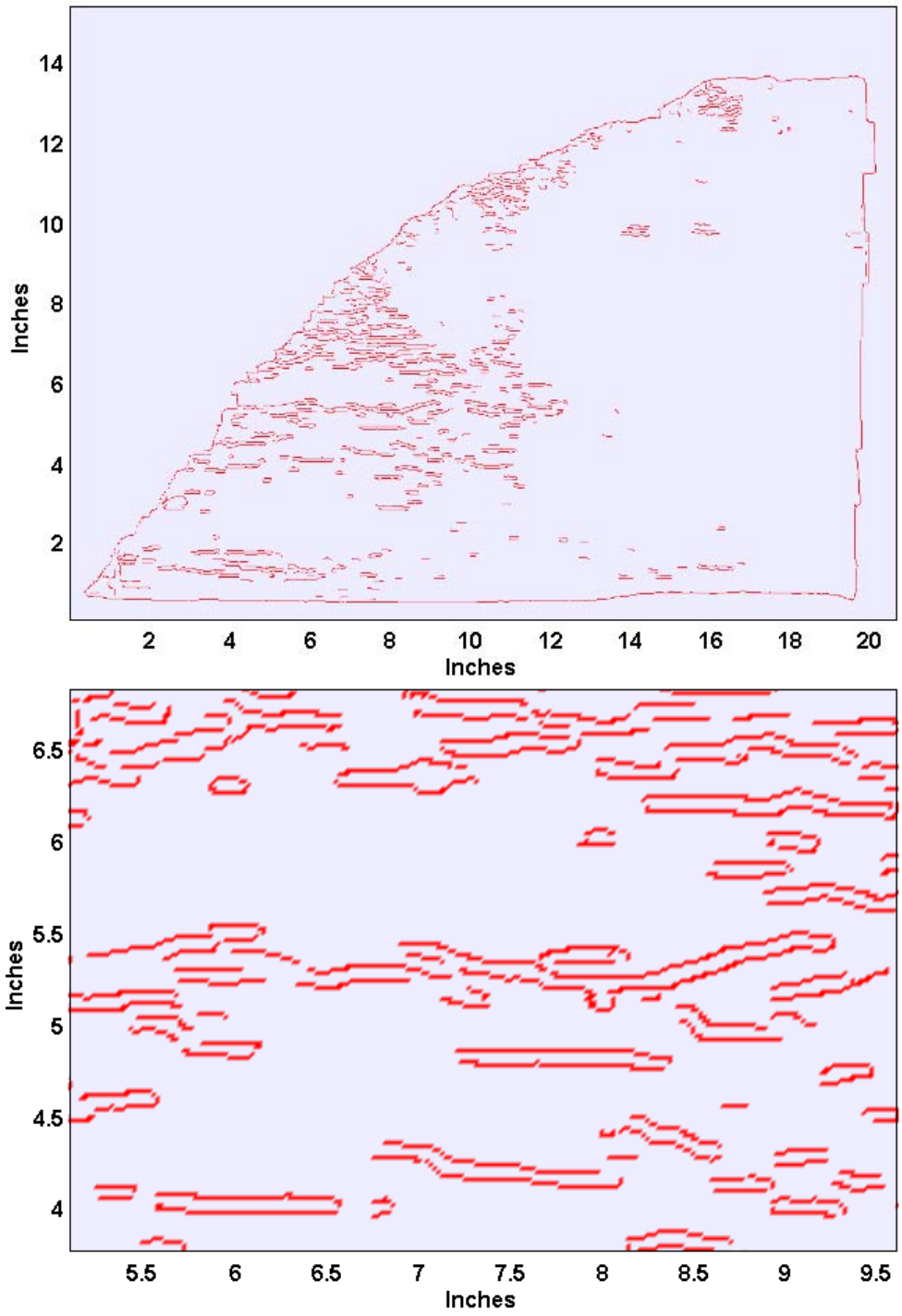

Figure 19. Processed measurement data using the Canny edge detection method. This method identifies regions with a high conductivity gradient.

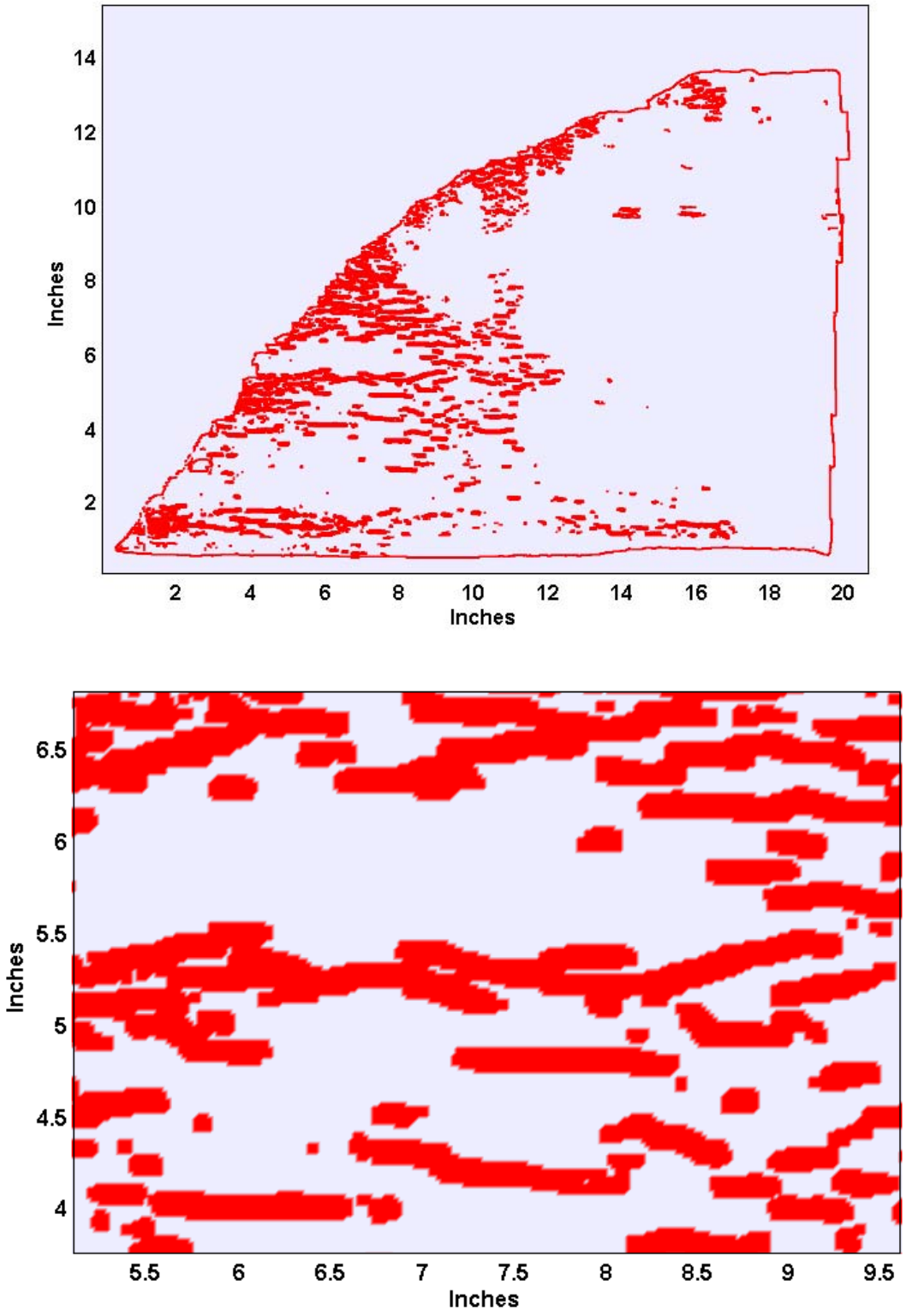

Figure 20. Hybrid processing method, which combines the Canny edge detection method with thresholded data.

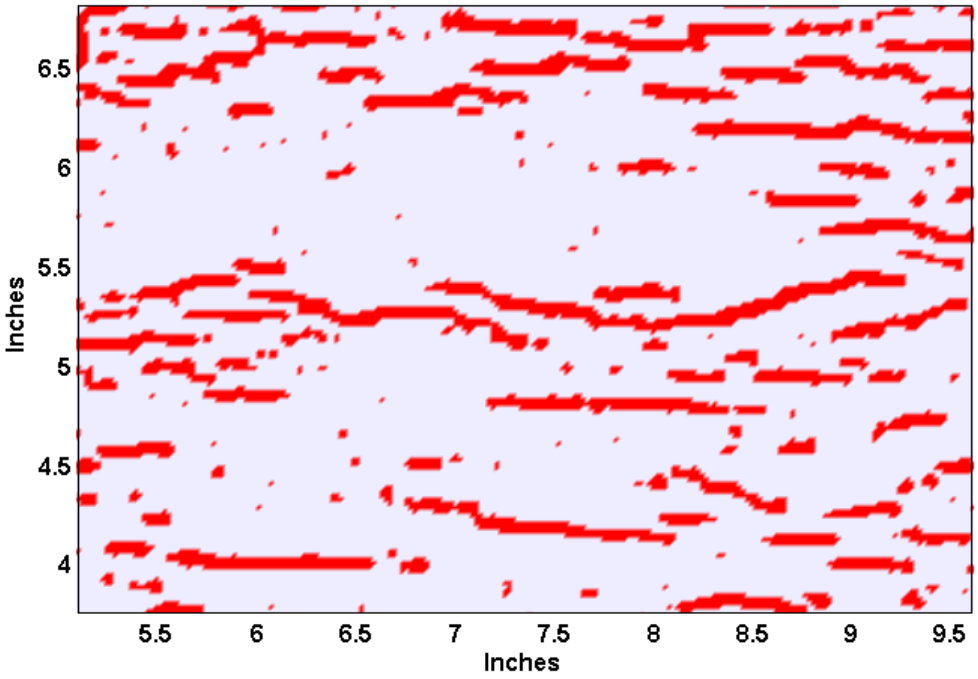

Figure 21. Thresholded high-pass filtered image; threshold = -0.05 (max).

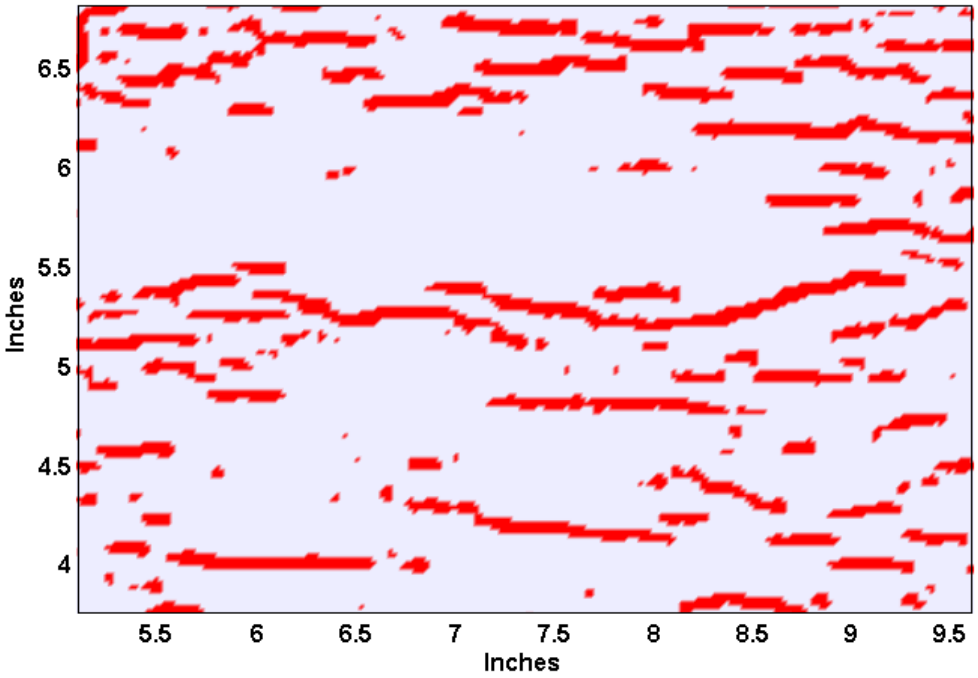

Figure 22. Thresholded high-pass filtered image; threshold = -0.12 (max).

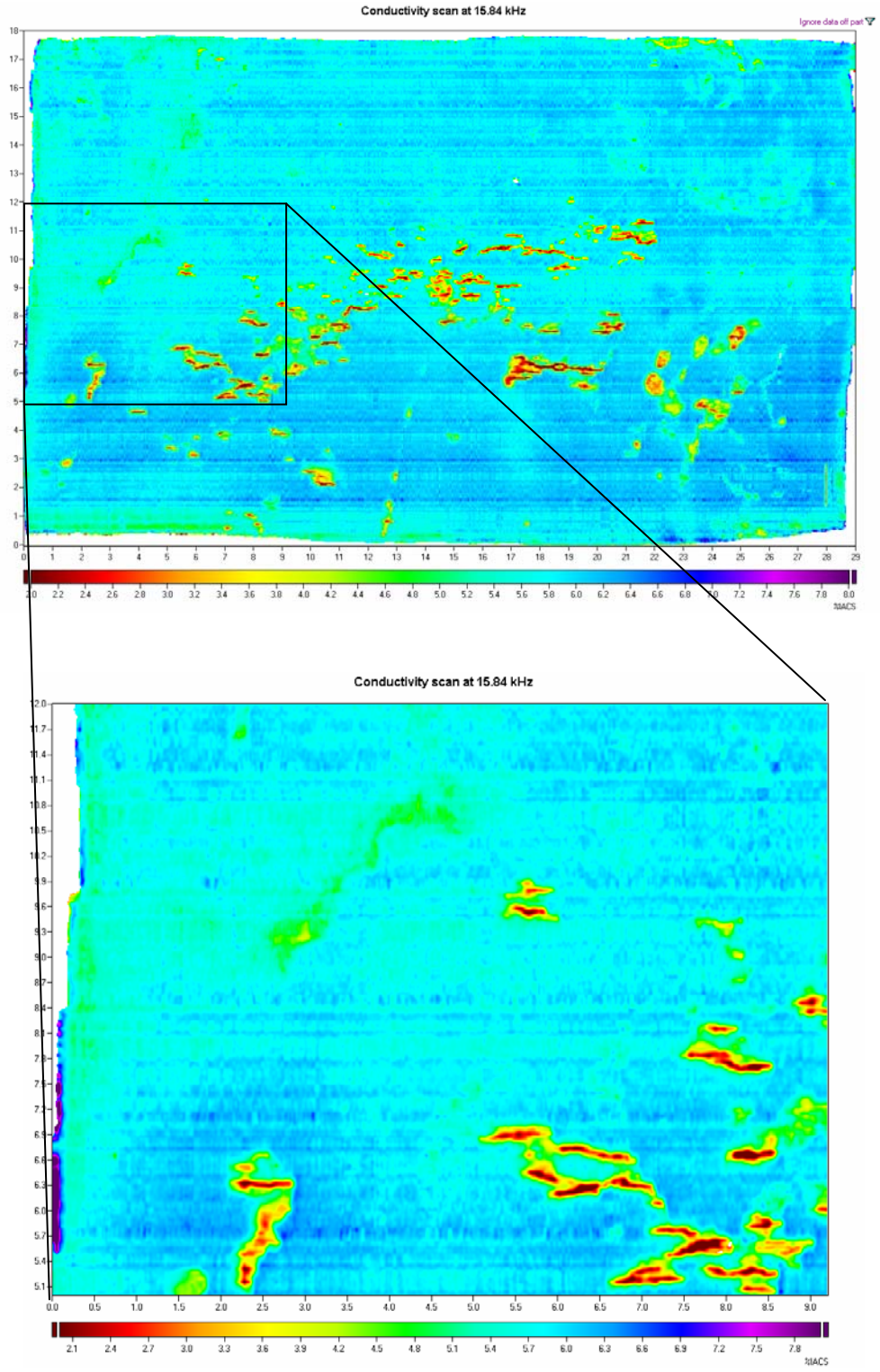

Figure 23. FA28 scan of Plate-01, at 15 kHz, showing region where the automatic crack identification and sizing algorithms were applied.

Table 1. Catalog of cracks present in the highlighted region of Figure 23, as automatically generated by the algorithms for crack identification and sizing. The table is sorted by axial crack length, and only cracks with an (arbitrarily established) axial length >0.010 in. are listed.

Location of crack start		Location of crack end		Axial	Crack	Location of crack center	
X coord.	Y coord.	X coord.	Y coord.	length (in.)	length (in.)	X coord.	Y coord.
5.92	6.08	7.18	6.12	1.26	1.26	6.59	6.19
7.54	7.74	8.59	7.60	1.05	1.06	8.07	7.67
6.01	6.63	6.94	6.50	0.93	0.94	6.51	6.59
7.78	5.24	8.65	5.20	0.87	0.87	8.21	5.21
6.67	5.08	7.51	5.14	0.84	0.84	7.08	5.15
5.12	6.75	5.95	6.71	0.84	0.84	5.59	6.81
7.30	5.41	8.08	5.57	0.78	0.79	7.71	5.49
2.15	6.24	2.90	6.24	0.75	0.75	2.53	6.23
5.42	9.37	6.01	9.33	0.60	0.60	5.71	9.41
8.05	6.54	8.62	6.59	0.57	0.58	8.33	6.58
7.15	5.67	7.69	5.65	0.54	0.54	7.43	5.67
5.45	9.59	5.98	9.65	0.54	0.54	5.73	9.63
7.72	8.01	8.17	8.05	0.45	0.45	7.94	8.05
8.26	5.73	8.68	5.77	0.42	0.42	8.47	5.77
5.63	6.36	6.04	6.26	0.42	0.44	5.85	6.33
8.68	5.41	9.07	5.55	0.39	0.41	8.86	5.46
8.38	5.51	8.74	5.55	0.36	0.36	8.55	5.52
8.89	8.35	9.22	8.39	0.33	0.34	9.05	8.36
7.81	9.29	8.11	9.23	0.30	0.31	8.00	9.24
2.42	5.53	2.72	5.55	0.30	0.45	2.56	5.70
2.24	5.43	2.54	5.45	0.30	0.30	2.40	5.43
8.98	8.23	9.25	8.23	0.27	0.27	9.11	8.23
2.21	6.44	2.42	6.42	0.21	0.21	2.32	6.43
8.86	7.07	9.04	7.13	0.18	0.24	8.97	7.14
2.69	5.85	2.87	5.93	0.18	0.26	2.79	5.95
8.23	5.35	8.38	5.37	0.15	0.16	8.30	5.36
7.15	6.00	7.30	5.96	0.15	0.16	7.23	6.00
5.80	6.48	5.95	6.44	0.15	0.16	5.89	6.47
2.45	6.56	2.60	6.56	0.15	0.15	2.53	6.57
2.27	5.12	2.42	5.24	0.15	0.32	2.34	5.18
1.68	5.22	1.83	5.12	0.15	0.18	1.77	5.17
8.11	8.94	8.23	8.88	0.12	0.14	8.18	8.90
7.69	7.85	7.81	7.85	0.12	0.12	7.73	7.87
5.60	9.72	5.71	9.72	0.12	0.13	5.67	9.73
2.96	9.07	3.08	9.11	0.12	0.13	3.02	9.11

If $y \le 0.14\dfrac{(\ell_1 + \ell_2)}{2}$

and $x \le 0.25\dfrac{(\ell_1 + \ell_2)}{2}$

Then cracks are interacting.

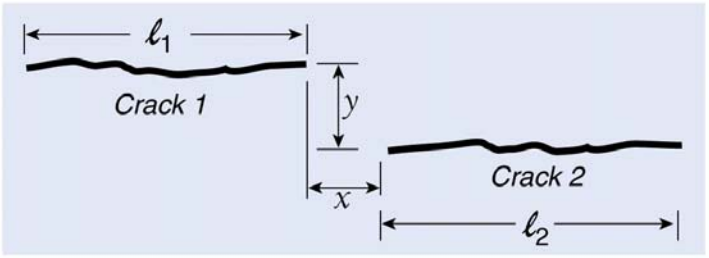

Figure 24. Guidance provided by ANSI/NACE Standard RP0204-2004, "Standard Recommended Practice, Stress Corrosion Cracking (SCC) Direct Assessment Methodology", uses dimensions of crack tip separation to determine which cracks are to be considered interacting.

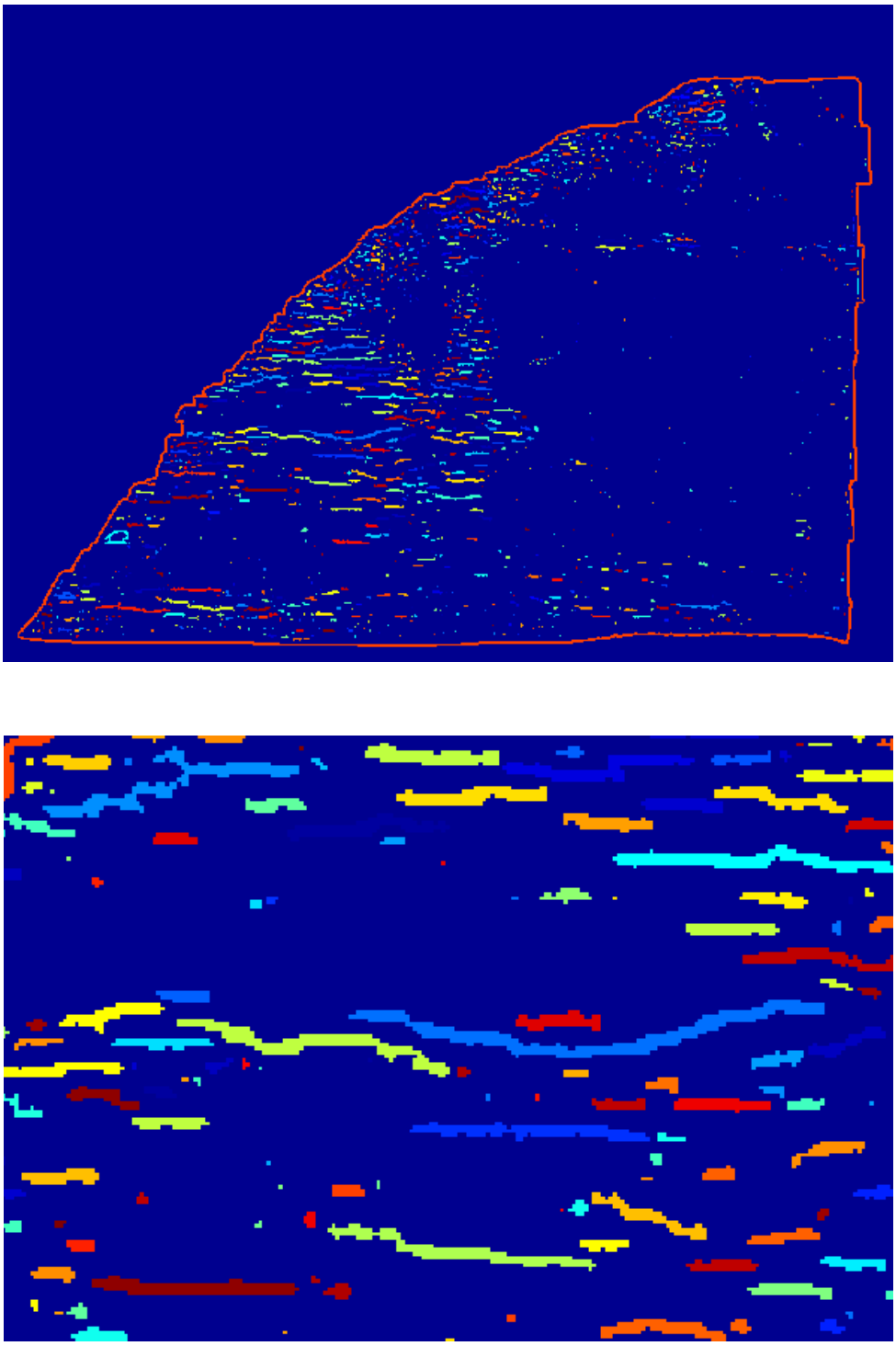

Figure 25. Connectivity algorithm using the threshold that was applied to the data shown in Figure 22. Each color corresponds to a crack that meets the algorithm's definition of a discrete crack.

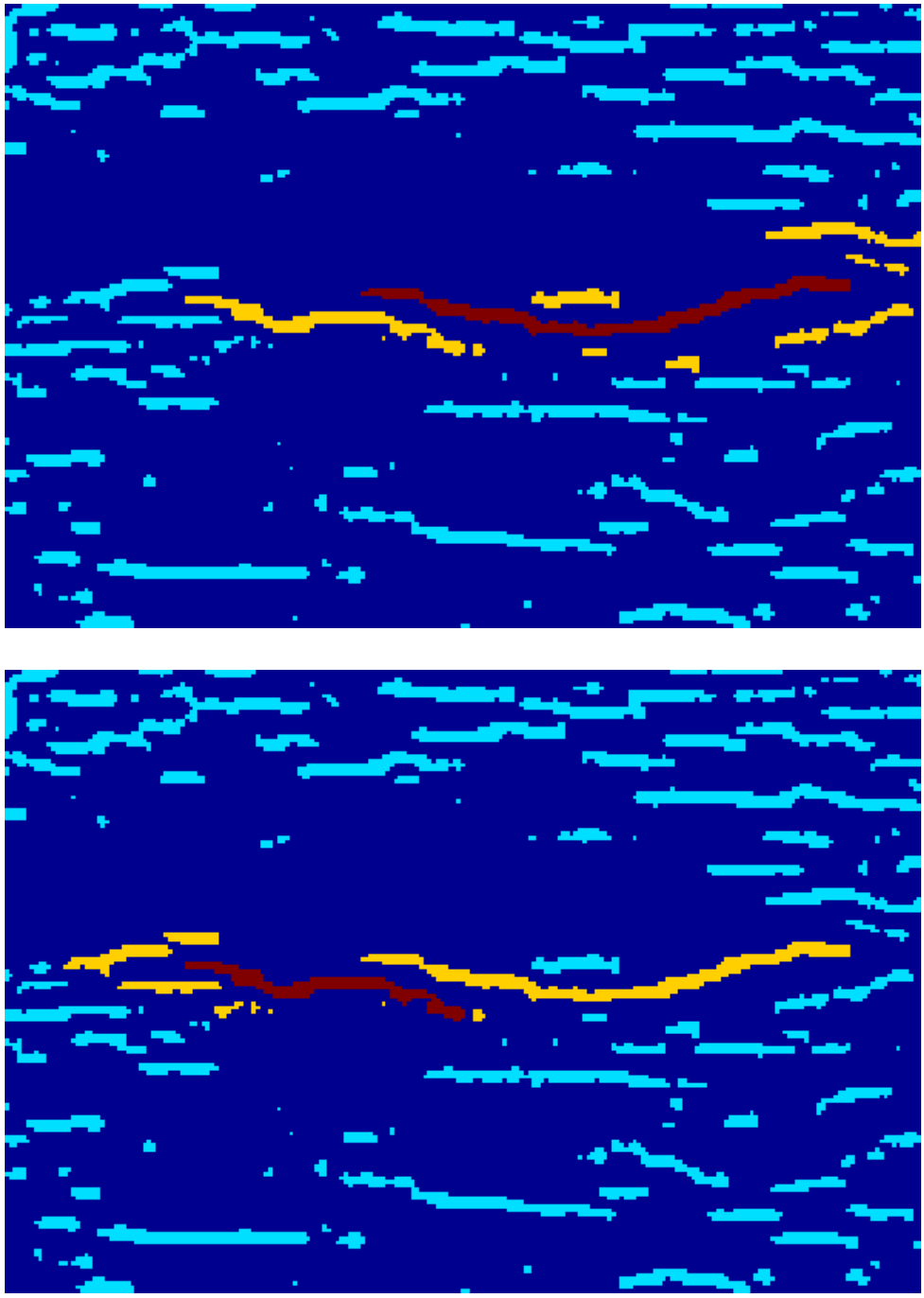

Figure 26. Two example outputs from the algorithm used for the detection of interacting cracks, applied to the data from Figure 25. In each figure the brown crack is the crack under consideration. The tan cracks are interacting with the brown crack, based on the criterion of Figure **24**.

Suppressing false indications

One feature on the surface of pipelines that must be accounted for when performing MWM-Array scans is the presence of "flash rust" on the surface. In FA28 scans at a drive frequency of 126 kHz, this flash rust was detected as a region of lower conductivity, as shown in Figure 31 (which is the upper left quadrant of the image shown in Figure 13). However, when this same region is scanned with an FA24 at a drive frequency of 10 kHz, the response from the flash rust is significantly reduced. These results show that, with the proper selection of sensor, frequency, and methods, this possible source of false indications can be suppressed.

Another important feature on pipelines that must be accounted for in MWM-Array scans is mechanical damage, which can include dents, gouges, and/or cold work caused by external mechanical impacts/forces. According to the Office of Pipeline Safety, failures for reportable incidents involving hazardous liquids and natural gas pipelines (transmission and distribution) are most commonly caused by mechanical damage. For hazardous liquids and gas transmission pipelines, mechanical damage follows corrosion as the leading cause of failure for reportable incidents. Mechanical damage may also occur as buckling, wrinkling or denting of the normal cross-section of the pipe, and include wall thinning due to radial and/or axial distortion. Changes in the local distribution of residual stresses can also occur due to mechanical damage, increasing the susceptibility to SCC. Since magnetic permeability is strongly stress dependent, JENTEK's MWM-Array sensors have the potential to locate and characterize mechanical damage in pipelines by imaging changes in wall thickness and permeability. This may be possible using high frequency MWM-Array methods that can map external SCC, external corrosion and residual stress distributions at the same time.

Separately we are investigating this application from pigging platforms to image internal corrosion and external mechanical damage (i.e., by imaging internal residual stresses), from the internal diameter. According to Carl Tores of Tuboscope and others, this alone would be a substantial contribution. Figure 33 shows the lift-off and permeability image from an MWM-Array FA24 sensor on a pipeline section with mechanical damage shown in Figure 32. The mechanical damage is captured by channel 13, 15 and 16 as indicated in blue on the right side of Figure 33.

The areas containing mechanical damage show a difference in permeability values compared to the region in green and blue. Most importantly the region in purple indicates tensile stresses near the mechanical damage sites that may increase susceptibility to SCC.

Figure 34 provides the lift-off and permeability responses for individual channels used to generate the images shown in Figure 33. These B-scans also show the increase in permeability associated with tensile stresses near the damage sites. Figure 35 shows the same data as in Figure 34 on a lift-off/ permeability measurement grid used to convert the data from raw transinductance into B-scans and images. The close-up view illustrates the variability in the lift-off and permeability directions, and the fact that the local variations are easily discriminated from the large volume of data away from the mechanical damage sites.

Also, we anticipate that the MWM-Array will be a valuable tool for assessing SCC at mechanical damage sites, as well as for assessing mechanical damage.

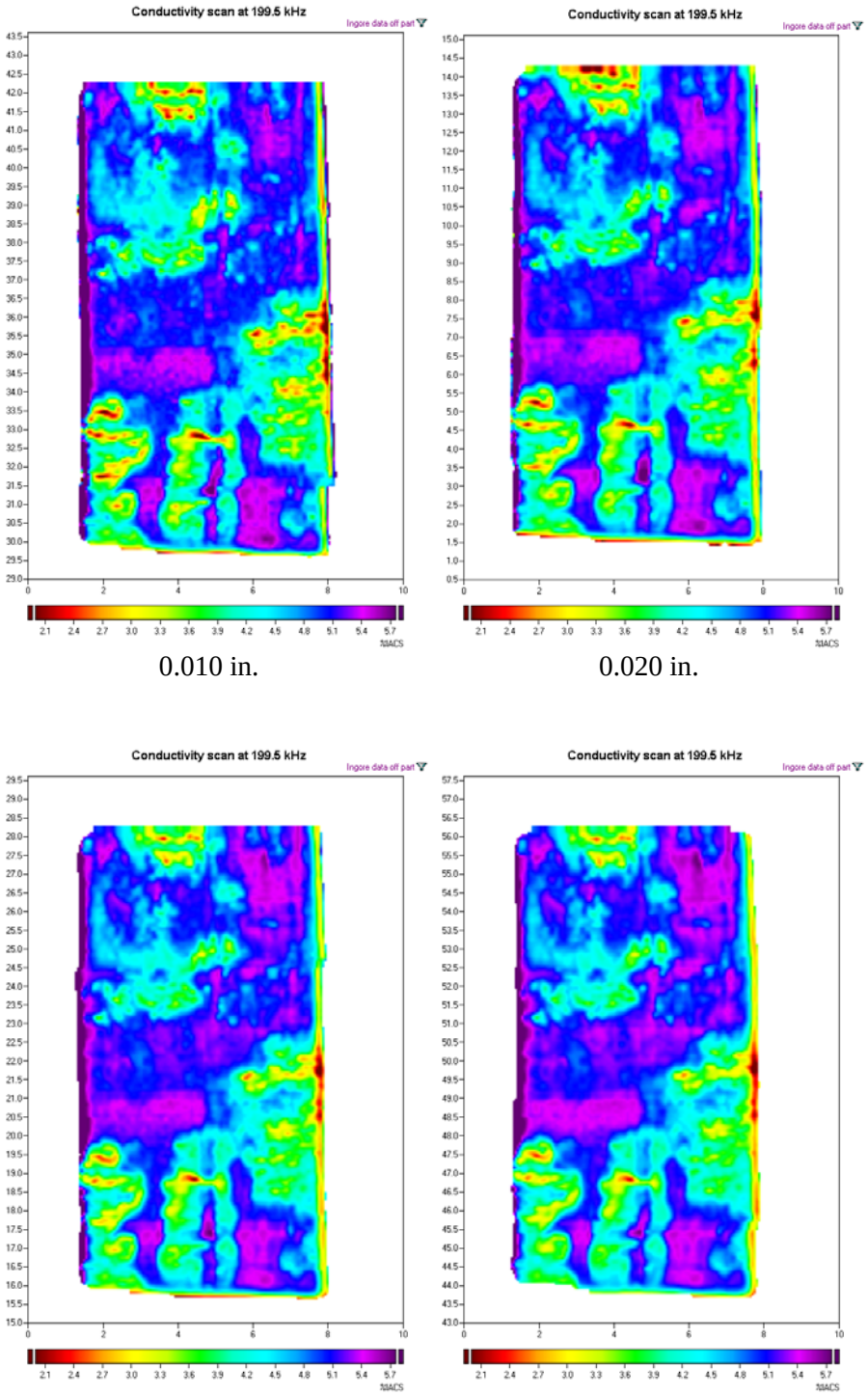

Figure 27. MWM-Array FA24 conductivity maps generated with 0.010 in., 0.020 in., 0.030 in., and 0.040 in. plastic shims placed between the plate and the sensor. There is little difference between the measurements acquired in this 0.010 – 0.040 in. lift-off range.

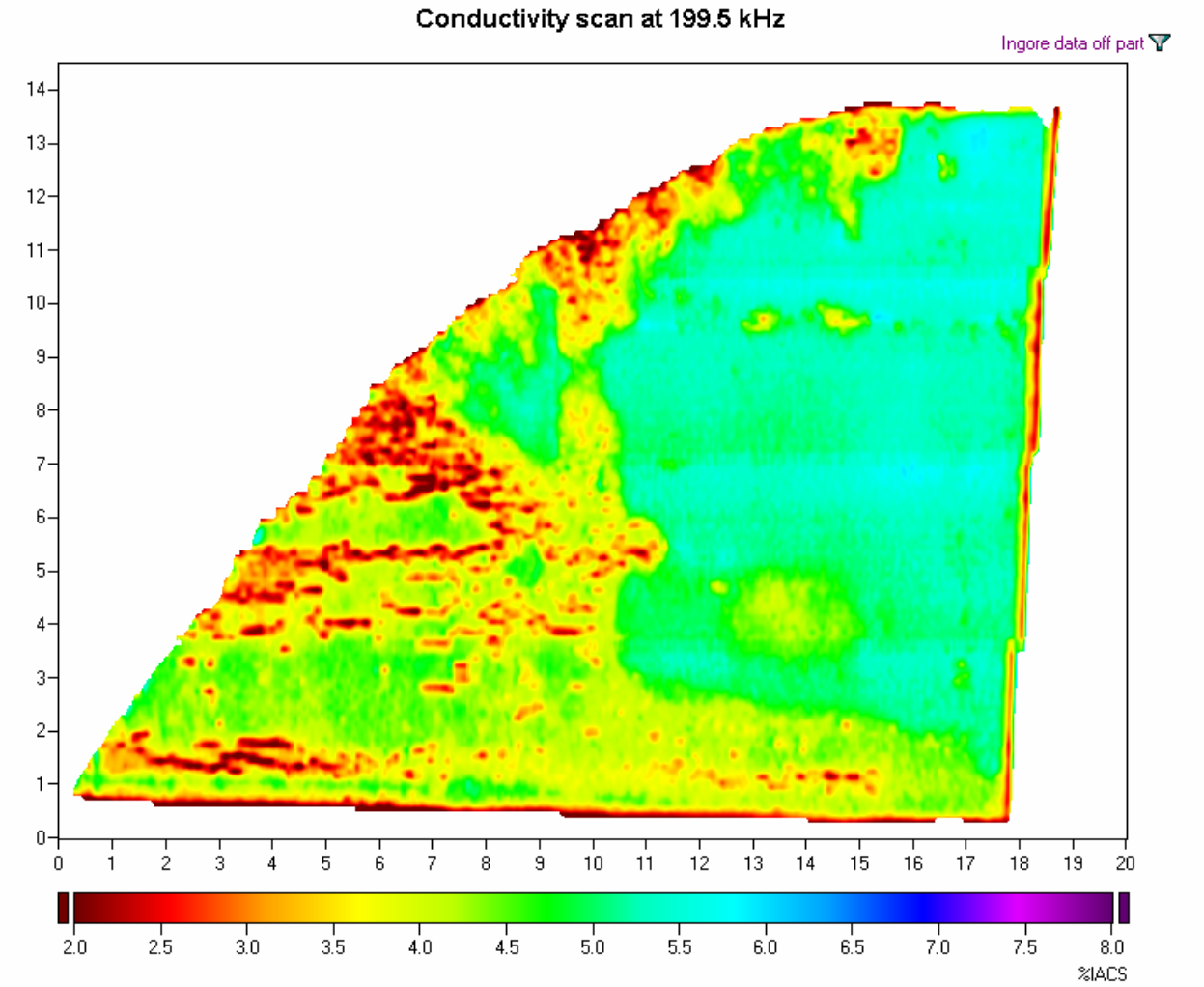

Figure 28. FA24 scan image of the triangular plate. The area can be scanned in about half the time as when a high-resolution FA28 sensor is used. All the SCC is detected, though because of the larger sensing elements of the FA24 many of the individual cracks are not resolved, i.e., they appear as one longer or wider crack.

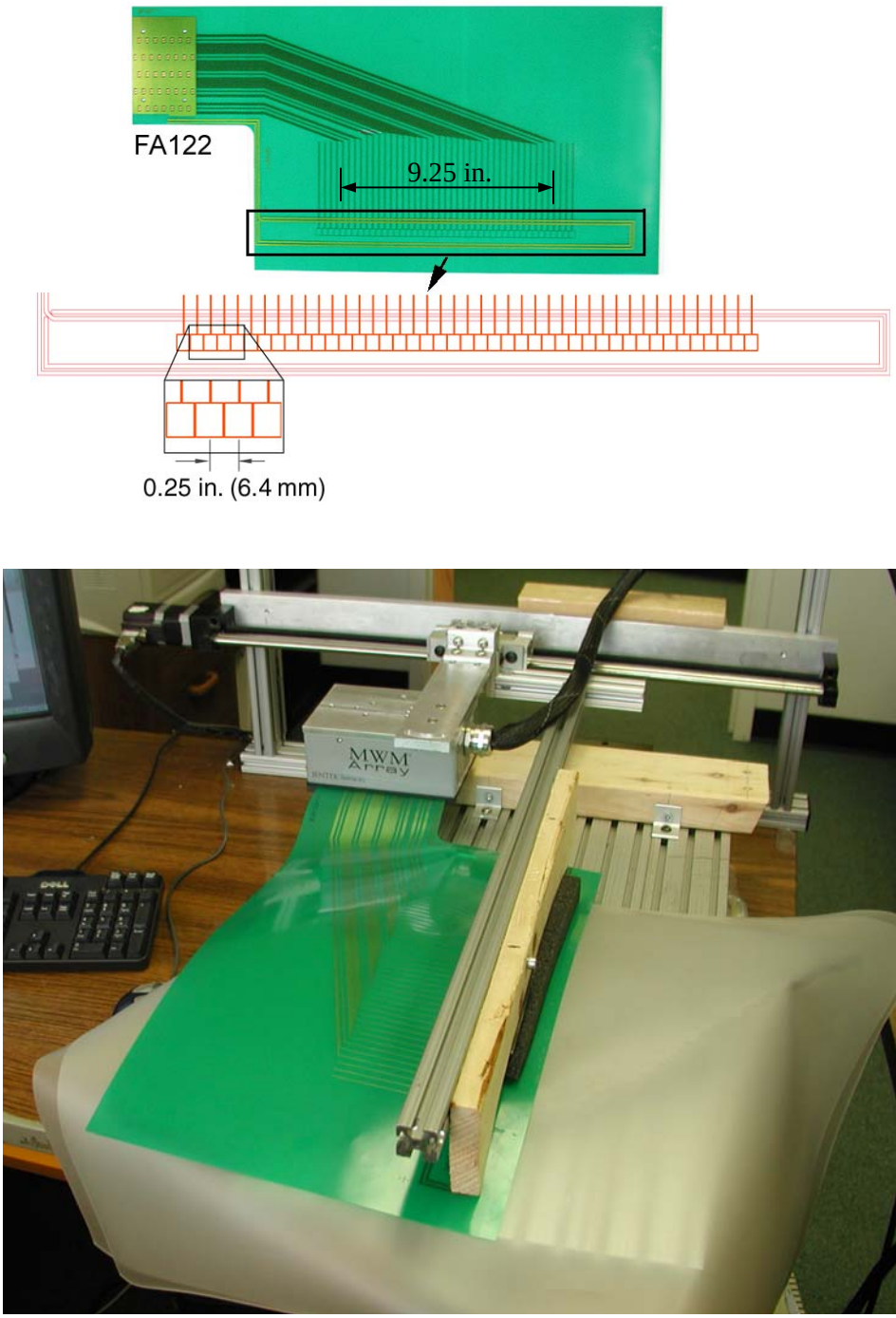

Figure 29. (Top) Photograph and schematic of the FA122 large linear array sensor originally designed as a deep penetration sensor for detecting far-surface corrosion in 0.125 in. thick aluminum. (Bottom) Photograph of the setup used to scan the triangular plate with the FA122.

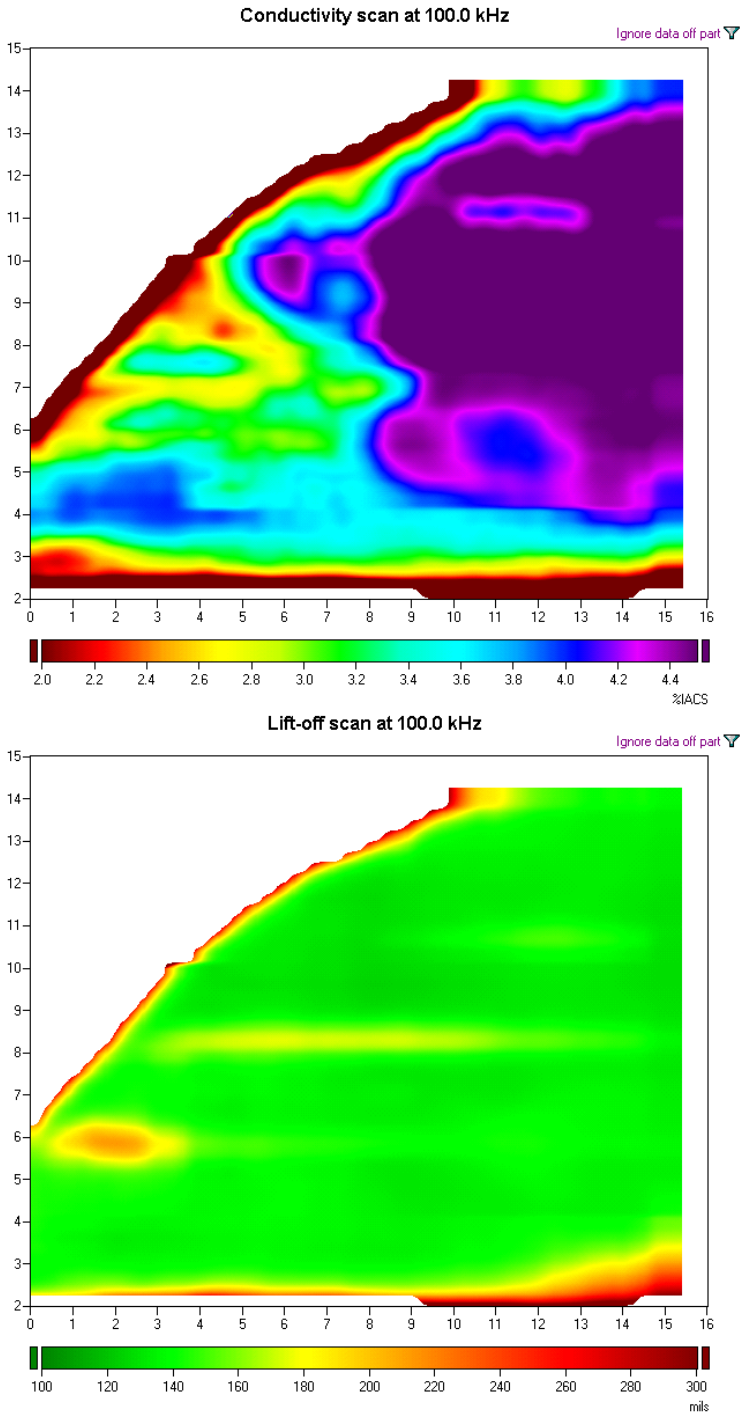

Figure 30. (Top) Conductivity and (bottom) Lift-off scan images from an FA122 scan of the triangular plate with 0.130 in. of shim between the sensor and the plate. The sensor, which was not designed for this application, detected the regions of SCC in the plate. The SCC regions are shown in red yellow, green, and blue in the conductivity image (note the edge effects also show up in these colors and should be ignored since pipeline sections inspected in the ditch will not typically have such edges).

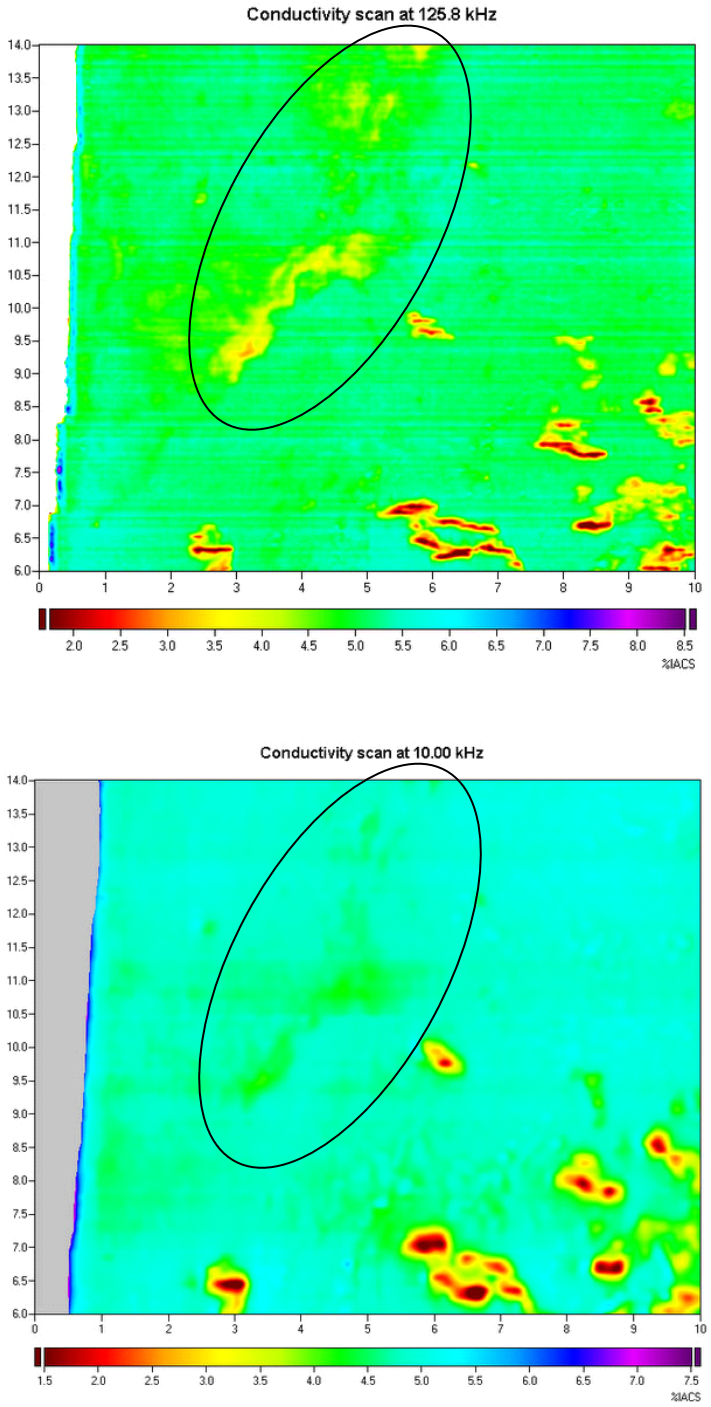

Figure 31. (Top) Conductivity scan image of a region in Plate-01 taken with an FA28 sensor at 125 kHz, and (bottom) image from the same region taken with an FA24 at 10 kHz. The sensor response from the "flash rust" region on the plate is significantly reduced in the FA24 image.

Figure 32. Photograph of mechanical damage on a pipeline section.

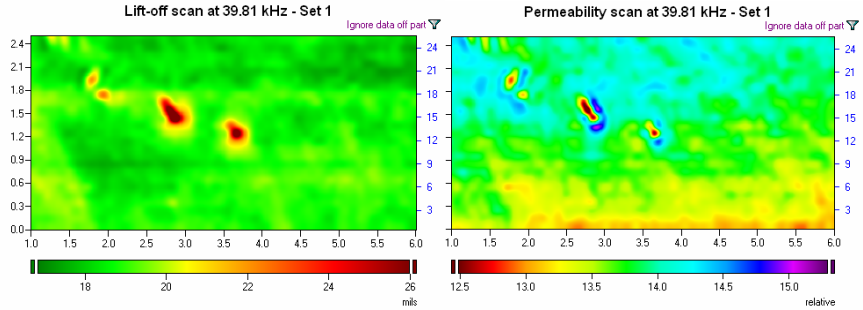

Figure 33. (left) Lift-off image from FA24 sensor. Small regions in red show a higher lift-off than regions in green. Red regions are the areas with mechanical damage. (right) Permeability image from the FA24 sensor.

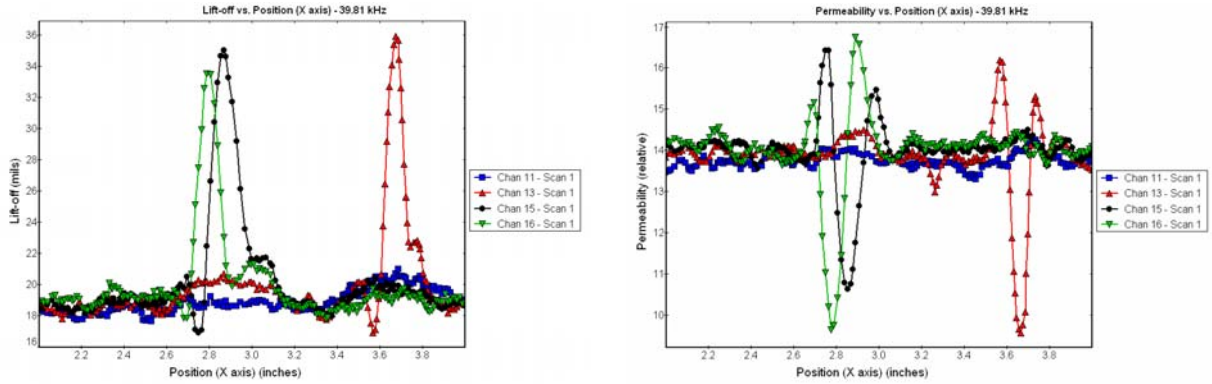

Figure 34. B-Scans (one dimensional plots) for lift-off and permeability.

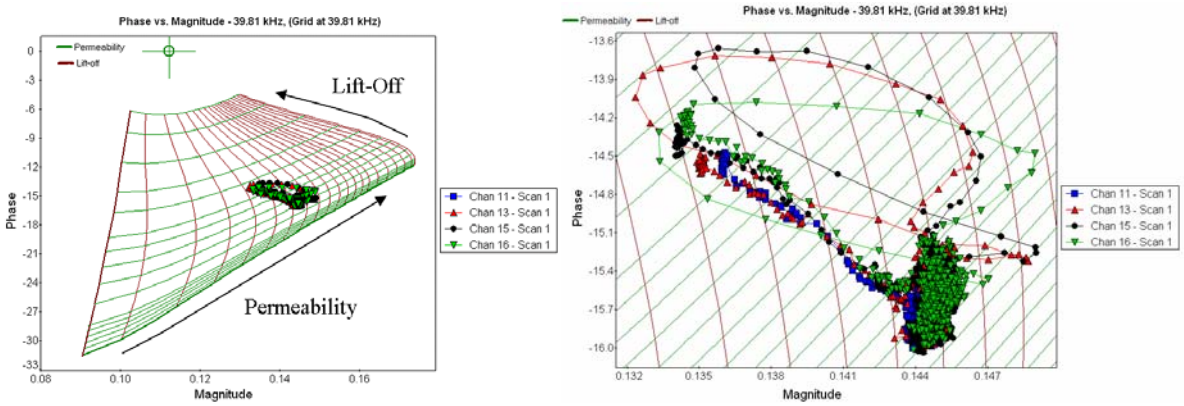

Figure 35. (Left) measurement data on the permeability – lift-off grid, and (right) a close-up of the same data.

Discussion on the characterization of coatings

The most common modes of failure in coatings are disbonding of the coating from the steel and holidays, i.e. holes in the coatings, that result from mechanical damage. Disbonding can occur from improper preparation of the steel surface prior to the application of the coating, or from a combination of a holiday in the coating, a breakdown in the cathodic protection system, and the introduction of moisture to the steel/coating interface. To detect such defects in the coating, it is expected that JENTEK's new magneto-thermography method could be used. Magneto-thermography is being developed under an ongoing NASA SBIR effort. This method replaces the IR camera with an MWM-Array to map electrical conductivities at the bond interface, potentially improving thermography capabilities for thick coatings.

Crack depth determination

As noted earlier, because there is currently no cost effective technology for the determination of crack depth, the industry instead relies on the more easily determined crack length., and uses grinding to determine crack depths. To investigate the MWM-Array capability to determine crack depth directly, 3D simulations were performed to determine the expected response of the FA28 to notch depth in a steel substrate. Figure 36 shows the basic simulation geometry. Current flows through the linear drive winding segment to create the magnetic field while the sense element responds to the proximity of the material under examination and the presence of the notch. The sense element shown is centered over a notch in the material surface. Symmetry is assumed to simplify the analysis and reduce the number of elements used in the numerical calculation. We will continue to investigate improved MWM-Array designs and crack depth estimation during the period between the end of Phase I and the recommended Phase II effort. Furthermore we continue to develop our lower frequency impedance instrumentation. As stated earlier this lower frequency capability is expected to be available to support the recommended Phase II effort.

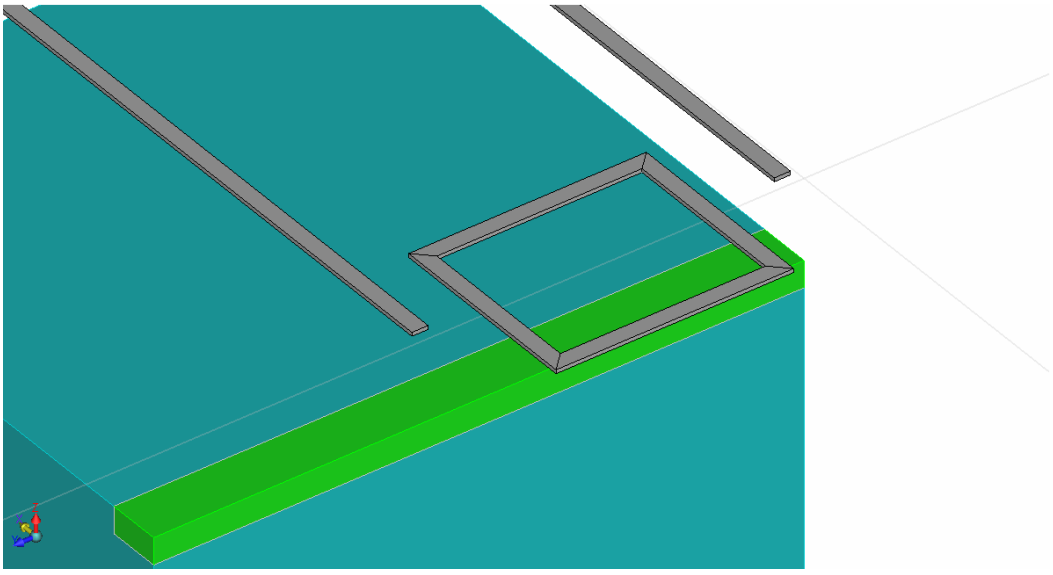

Figure 36. Simulation geometry for a half of an FA28 over a notch in a steel.